A spatially constrained independent component analysis jointly informed by structural and functional network connectivity.

Mahshid Fouladivanda[1,2]*, Armin Iraji[1,2], Lei Wu[1], Theodorus G.M. van Erp[3], Aysenil Belger[4], Faris Hawamdeh[6], Godfrey D. Pearlson[5], Vince D. Calhoun[1,2]*

[1] Tri-institute Translational Research in Neuroimaging and Data Science (TReNDS Center), Georgia State University, Georgia Institute of Technology, Emory University, Atlanta, GA, USA.
[2] Georgia State University, Atlanta, GA, USA.
[3] Clinical Translational Neuroscience Laboratory, Department of Psychiatry and Human Behavior School of Medicine, University of California, Irvine, CA, USA.
[4] Department of Psychiatry Director, Neuroimaging Research in Psychiatry Director, Clinical Translational Core, UNC Intellectual and Developmental Disabilities Research Center, University of North Carolina, Chapel Hill, NC, USA.
[5] Olin Neuropsychiatry Research Center, Department of Psychiatry and Neuroscience, Yale University, School of Medicine, New Haven, CT, USA.
[6] Center for Disaster Informatics and Computational Epidemiology (DICE), Georgia State University, Atlanta, GA, USA.

Abstract

There are a growing number of neuroimaging studies motivating joint structural and functional brain connectivity. Brain connectivity of different modalities provides insight into brain functional organization by leveraging complementary information, especially for brain disorders such as schizophrenia. In this paper, we propose a multi-modal independent component analysis (ICA) model that utilizes information from both structural and functional brain connectivity guided by spatial maps to estimate intrinsic connectivity networks (ICNs). Structural connectivity is estimated through whole-brain tractography on diffusion-weighted MRI (dMRI), while functional connectivity is derived from resting-state functional MRI (rs-fMRI). The proposed structural-functional connectivity and spatially constrained ICA (sfCICA) model estimates ICNs at the subject level using a multi-objective optimization framework. We evaluated our model using synthetic and real datasets (including dMRI and rs-fMRI from 149 schizophrenia patients and 162 controls). Multi-modal ICNs revealed enhanced functional coupling between ICNs with higher

1

36   structural connectivity, improved modularity, and network distinction, particularly in

37   schizophrenia. Statistical analysis of group differences showed more significant differences in the

38   proposed model compared to the unimodal model. In summary, the sfCICA model showed benefits

39   from being jointly informed by structural and functional connectivity. These findings suggest

40   advantages in simultaneously learning effectively and enhancing connectivity estimates using

41   structural connectivity.

42

43   Keywords: multi-modal independent components analysis, multi-objective model, diffusion MRI,

44   resting state fMRI, spatial constraint, schizophrenia

45
46   Corresponding authors: Mahshid Fouladivanda (mfouladivanda@gsu.edu),
47   Vince. D. Calhoun (vcalhoun@gsu.edu)

1. Introduction

The human brain can be modeled as a distinct functional unit that exhibits a temporally synchronized pattern known as intrinsic connectivity networks (ICNs) (Genon et al., 2018; Iraji et al., 2020). These ICNs interact with each other, collectively representing brain function. Consequently, accurate estimation of ICNs is a critical step in studying brain networks because it minimizes the impact of inaccuracies in functional activities (Iraji et al., 2020). One approach for identifying ICNs and gaining insights into brain networks, including brain disorders like schizophrenia (Iraji et al., 2019; Iraji, Faghiri, Fu, Kochunov, et al., 2022; Iraji, Faghiri, Fu, Rachakonda, et al., 2022), is data-driven independent component analysis (ICA) (Calhoun & Adalı, 2012; Calhoun & de Lacy, 2017). This method assumes spatial independence for the temporally synchronized functional units and recovers a set of maximally independent sources from a mixture of unknown source signals without any prior information (Calhoun et al., 2001), using single modality neuroimaging, particularly resting-state functional magnetic resonance imaging (rs-fMRI). Rs-fMRI images dynamically measure the hemodynamic response associated with neural activity in the brain during rest.

ICA has become widely used to partition the brain into spatially overlapping and distinct ICNs at the group level. Group ICNs are estimated using fMRI images from all subjects, then the corresponding subject-level ICNs are obtained. The most common approach is to apply ICA to the data, then use back reconstruction to estimate subject-specific maps (Allen et al., 2011; Calhoun et al., 2001; Erhardt et al., 2011). These approaches are fully data-driven; however, more recently, spatially constrained ICA approaches (Du & Fan, 2013; Lin et al., 2010) have been proposed to estimate ICNs using a set of templates for ICNs as priors. They can be used to build a fully

70   automated approach (e.g., the NeuroMark pipeline (Du et al., 2020)) that does not require post hoc

71   ICN selection or network matching (Du et al., 2020), and also automatically provides ICN

72   ordering, providing modular functional network connectivity. These approaches have been used

73   in many prior studies and offer a fully automated framework that can be integrated within a larger

74   framework (e.g., a containerized version is available from http://trendscenter.org/software/gift, as

75   well as a BIDSapp (Kim et al., 2023)), making them more easily comparable across studies.

76   Current constrained ICA approaches are unimodal and do not leverage information from other

77   modalities, particularly dMRI images. Although MRI images, such as T1 and T2, include structural

78   information about the brain, dMRI images provide information about the physical paths in the

79   human brain, captured as structural connectivity which drives functional activities of different

80   units. In this study, we investigate a model that estimates functional brain patterns (ICNs) informed

81   by multi-modal data to provide a more complete view of the connectome by employing both

82   structural and functional connectivity. This has many advantages, for example, a connectivity

83   domain ICA approach (Iraji et al., 2016) called joint connectivity matrix ICA has been used to

84   jointly parcellate structural and functional connectivity data, yielding a data-driven

85   structure/function parcellation (Wu & Calhoun, 2023).

86   One longstanding aspiration in brain research is to link brain function to its underlying architecture,

87   making the interplay between structural connectivity and functional network connectivity (FNC)

88   a fundamental in network neuroscience (Park & Friston, 2013). There have been studies, such as

89   (Calhoun & Sui, 2016) using computational models on the connectivity domain to estimate the

90   human brain functional activities propounding from different modalities, mainly single modality

91   information. Consequently, a fundamental question arises regarding how to model human brain

92   functional activity changes with a deeper understanding of structural and functional information

93   (Batista-García-Ramó & Fernández-Verdecia, 2018; Skudlarski et al., 2010). Several studies have

94   been proposed to fill this gap ((Batista-García-Ramó & Fernández-Verdecia, 2018; Suárez et al.,

95   2020)) by developing different models predicting FNC from structural connectivity using

96   statistical models (Messé et al., 2014; Mišić et al., 2016; Suárez et al., 2020), or communication

97   models based on structural-functional network connectivity (Goñi et al., 2014; Zamani Esfahlani

98   et al., 2022).

99   In addition, jointly analyzing models is a growing methodology used to investigate the human

100   brain and how structural and functional relate to each other (Calhoun & Sui, 2016; Puxeddu et al.,

101   2022; Zhu et al., 2021). One may provide variations in brain functions at different regions by

102   multilayer network models (Puxeddu et al., 2020; Shine et al., 2016). Multilayer network models

103   have emerged to analyze the human brain employing the concepts of graph theory with multiple

104   viewings of the human brain (Puxeddu et al., 2020; Puxeddu et al., 2022). In parallel, other studies

105   have investigated brain network modules, uncovering intrinsic brain network activations using

106   data-driven models (Calhoun & Adalı, 2012; Yeo et al., 2011), and community detection (Power

107   et al., 2011). Several studies have attempted to develop multi-modal fusion models (Calhoun &

108   Sui, 2016; Sui et al., 2014) incorporating complementary information across modalities into the

109   analysis of ICNs (Batista-García-Ramó & Fernández-Verdecia, 2018; Suárez et al., 2020). Multi-

110   modal fusion can provide additional insights into brain structure and function that are impacted by

111   psychopathology, including identifying which structural or functional aspects of pathology might

112   be linked to human behavior or cognition (Sui et al., 2014), particularly in disorders related to both

113   brain function and structures such as schizophrenia (Calhoun, 2018).

114   Moreover, information from different modalities can be jointly analyzed to investigate ICNs using

115   ICA. This has been done mostly by focusing on linking group-level spatial features, including joint

116   ICA (jICA) (Calhoun et al., 2006), parallel ICA (pICA) (Liu et al., 2009), parallel ICA with

117   reference (pICAR) (Chen et al., 2013), multi-modal canonical correlation analysis (mCCA)+jICA

118   (Sui et al., 2011), multisite canonical correlation analysis with reference (mCCAR)+jICA (Qi et

119   al., 2018; Shile et al., 2016), and linked ICA (Groves et al., 2011), or jointly optimizing for fMRI

120   networks and covarying networks from structural MRI as in parallel group ICA+ICA.

121   However, these approaches have not directly integrated structural and functional network

122   connectivity information (Qi et al., 2022; S. L. Qi et al., 2019). To our knowledge, fewer prior

123   works have used structural connectivity to estimate ICNs, as in (Wu & Calhoun, 2023), which

124   performed joint structure/functional parcellation. Specifically, there is a lack of methodologies to

125   guide adaptive ICN estimation by incorporating both structural and functional network

126   connectivity. A common practice in neuroscience is to compress Network connectivity

127   information into nodes and edges to understand functional interactions in the brain

128   (Babaeeghazvini et al., 2021). Thus, using network connectivity helps to drive the model to learn

129   from both structural connectivity (real connections among different functional networks) and FNC

130   (their functional interactions).

131   In this paper, we introduce a novel adaptive ICA model designed to directly investigate the ICNs.

132   This is achieved by imposing constraints using two different modalities at the subject level. Our

133   approach involves constructing a new multi-modal ICA model that jointly embeds structural and

134   functional network connectivity. This model is supported by previous studies that indicate that

135   structural connectivity forms the foundation of functional connectivity (Honey et al., 2009;

6

136 Litwińczuk et al., 2022; Stam et al., 2016; Zhu et al., 2021). In addition, we incorporated prior

137 spatial information into our multi-modal ICA model to increase the generalizability of the

138 estimated ICNs. Our model is an iterative pipeline that simultaneously learns from both dMRI and

139 fMRI, along with ICN spatial maps, to identify joint structural-functional independent

140 components.

141 While prior work (Wu & Calhoun, 2023) applied a connectivity-based model to perform joint data-

142 driven parcellation of dMRI and fMRI, no approaches have attempted to directly link the full

143 spatiotemporal fMRI data with dMRI data in the context of a connectivity constraint at the subject

144 level within a spatially constrained model, thus providing a fully automated approach. Our

145 proposed structural-functional network connectivity and spatially constrained ICA model

146 (sfCICA) identifies ICNs that are simultaneously optimized to be maximally spatially independent,

147 influenced by both structural and functional connectivity. Thus, the learning procedure to estimate

148 subject-level ICNs is informed by the structural and functional network connectivity information

149 of each subject. We first validated the approach employing synthetic data and then applied the

150 proposed model to a real dataset, including controls and patients with schizophrenia. The results

151 demonstrate that the proposed method can effectively impose prior information on ICNs while

152 jointly learning from structural-functional network connectivity in both synthetic and real human

153 brain data. Furthermore, the identified ICNs exhibit an increased ability to distinguish between

154 healthy controls and individuals with schizophrenia.

155

156

157 ## 2. Material and Methods

158 **2.1. Structural-functional network connectivity and spatially constrained ICA (sfCICA).**

159 **Model definition.**

160 A multi-modal ICA (sfCICA) model, called *structural and functional network connectivity and*

161 *spatially constrained ICA* was introduced. Briefly, the sfCICA framework estimates subject-level

162 ICNs by imposing structural network connectivity weights on time course distances (functional

163 network connectivity). The main advantage of the constraints in the sfCICA framework is driving

164 the model to jointly learn from both structural and functional network connectivity at the subject

165 level. Using the sfCICA model, subject-specific ICNs were estimated through multi-modal

166 information, incorporating prior spatial maps for each ICN derived from a standard template.

167 In summary, we introduced a multi-objective function as described in **Eq. 1**, consisting of three

168 terms. The first and second terms find independent ICNs which are learned from the spatial

169 template. The third term constrains the learning procedure to account for both structural and

170 functional network connectivity.

$$\max \quad (J(S_l^k), F(S_l^k), -C(w_l^k)) \tag{1}$$

$$\text{s. t. } \left\| w_l^k \right\|^{\square} = 1$$

171

172 The sfCICA model was proposed in a multi-objective framework, aiming to estimate ICNs by

173 optimizing their independence, through maximizing their non-Gaussianity measured by

174 negentropy or kurtosis ($J(S_l^k)$) (Hyvarinen, 1999) (**Eq. 2**).

$$\max \quad J(S_l^k) = (E[G(S_l^k)] - E[G(v)])^2 \tag{2}$$

$$\text{s. t. } \left\| w_l^k \right\|^{\square} = 1$$

175

176 Where, G is any quadratic function, E is the expectation maximization operator, and v is a random

177 variable. S_l^k and w_l^k are respectively the spatial map and time course of the lth ICN (here we use

178 Neuromark_fMRI_1.0 including 53 ICNs) for k^{th} subject. These are estimated by maximizing the

179 square differences between the expectation maximization of two vectors, as defined in **Eq. 2**.

180 In addition, the similarity of the spatial maps with the prior spatial information was maximized by

181 another cost function $(F(S_l^k))$ in **Eq. 3**. Thus, independence and similarity to the prior spatial

182 information (here a standard template was used) were jointly maximized during optimization.

$$\max \quad F(S_l^k) = E[S_l S_l^k] \tag{3}$$

$$\text{s. t. } \left\| w_l^k \right\|^{\square} = 1$$

183

184 where the S_l denoted the spatial map of the lth components in the template.

185 Furthermore, we integrate structural connectivity information, measured as the number of

186 streamlines connecting node pairs, into the model as a constraint on the FNC of the estimated time

187 course. To this end, the model is guided by minimizing the weighted distances of the time courses

188 based on structural connectivity. The structural connectivity weights captured from dMRI can

189 reflect existing physical connectivity between functionally related gray matter regions, this means,

190 more fiber bundles between two brain regions (here are ICNs) may result in stronger functional

191 correlations and shorter distances between time courses (Zhu et al., 2021).

192 Thus, we assumed regions with higher structural connectivity (more fiber tracts) would exhibit

193 closer functional signal activities because of their shorter distance. Prior works (He & Niyogi,

194 2003; Zhu et al., 2021), led us to reconstruct an objective function $(\min \sum_{ji}^{\square} M_{lj} \left\| FC_i^{\square} - FC_j^{\square} \right\|^2)$

195 to adjust the functional activity of an ICN by considering other structurally connected ICNs. Here,

196 M_{lj} represents structural connectivity weights and FC denotes the correlation between pairs of

197   ICNs (l, j). It is important to note that maximizing the FC between ICNs involves minimizing the

198   distance of their time courses. Therefore, we propose the following cost function (**Eq. 4**), in

199   addition to the previous cost functions, to be simultaneously optimized. This is aimed at

200   incorporating information from both structure and function as constraints.

$$\min \quad L\left(w_l^{\square}\right) = \sum_{j=1}^{L} M_{lj} \left\| w_l^k - w_j^k \right\|^2 \tag{4}$$

$$\text{s. t. } \left\| w_l^k \right\|^{\square} = 1$$

201

202   To solve a multi-objective optimization problem, one usually needs to find the Pareto optimal set

203   or its subset and critically evaluate which specific trade-off is more appropriate to the problem

204   under study. In addition, optimizing a linear weighted sum of cost functions is a commonly used

205   method for solving multi-objective optimization problems, which simplifies the problem

206   (Klamroth & Jørgen, 2007). In our study, we utilize a linear weighted approach to address the

207   multi-objective problem described in **Eq. 1.** This allows us to explore various points along the

208   Pareto front by adjusting the weighting values in the linear weighted sum objective function.

$$C = \alpha J\left(S_l^k\right) + \beta F\left(S_l^k\right) - \gamma L\left(w_l^k\right) \tag{5}$$

$$\text{s. t. } \left\| w_l^k \right\|^{\square} = 1$$

209

210   Where, α, β , and γ are constant weight values. To ensure a fair comparison and prevent the

211   optimization from being biased towards a cost function with a larger magnitude, we normalize the

212   cost functions in **Eq. 2-4** as described in (Du & Fan, 2013), and weights (α, β, and γ) are chosen

213   to be equal (0.33). Then a gradient ascent method was used to iteratively converge on an optimal

214   solution. The iterative algorithm for optimizing the cost (C) is derived as follows. Initially, $S_l^k =$

215     $\left(w_l^k\right)^T * X^k, S_l^k$, is substituted into **Eq. 6**.

10

$$C(w_l^k) = \alpha J(w_l^k) + \beta \, F(w_l^k) - \gamma L(w_l^k) \tag{6}$$

216

217   Then, according to the derivatives of each term, we have:

$$\nabla C(w_l^k) = \alpha \nabla J(w_l^k) + \beta \, \nabla F(w_l^k) - \gamma \nabla L(w_l^k) \tag{7}$$

218

219   More details regarding the derivative of each term are described in (Du & Fan, 2013). Once the

220   gradient of the objective function of **Eq. 7** is available, we employ the steepest ascent iterative

221   formula:

$$[w_l^k]^{t+1} = [w_l^k]^t + \mu^t . d^t \tag{8}$$

222

223   Where $[w_l^k]^{t+1}$ represents the value of w_l^k after t+1 iteration, d^t is the normalized $\nabla C(w_l^k)$ and,

224   μ^t stands for the step-length. To ensure a sufficient increase in the objective function in an inexact

225   line search, μ^t was estimated using the Armijo condition (Jorge Nocedal, 2006).

226   **2.2. Evaluation analysis.**

227   To evaluate the benefit of leveraging multi-modal information, we compare our model with one

228   of the spatial constrained ICA (CICA) models, known as a multi-objective optimization ICA

229   model (Du et al., 2020), which is a simplified version of the proposed framework when the multi-

230   modal information is not utilized. To this end, first, we used synthetic data to confirm that the

231   model is working in the intended objective defined for the optimization of the time series. Then,

232   we cope to evaluate our hypothesis using real data, capturing better group differences by

233   leveraging multi-modal information.

234   **2.2.1. Synthetic data**

235   **Simulation.** The synthetic dMRI was from FiberCup phantom data (Fillard et al., 2011; Poupon

236   et al., 2008) (https://tractometer.org/fibercup/data/), including 3mm isotropic images in 64

237   uniformly distributed over a sphere with b-value = 2000 m/s. It also provided 16 brain regions and

11

238   fiber pathways among the regions to reconstruct structural connectivity, (shown in **Figure 1**). To

239   keep consistency between the simulated dMRI and fMRI data, we used the same sixteen predefined

240   FiberCup regions as a reference to design synthetic fMRI images, similar to (Chu et al., 2018). We

241   simulated synthetic fMRI images using the simTB toolbox (Erhardt et al., 2012),
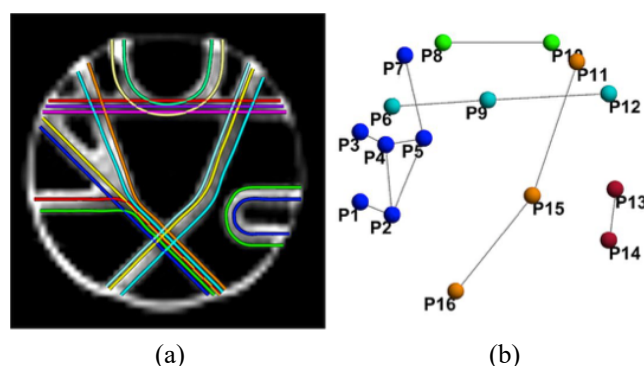
242   (https://trendscenter.org/software/simtb/).

243

(a)   (b)

Figure 1. In panel (a) and (b), we present simulated fiber pathways and predefined regions from FiberCup, respectively, for the reconstruction of synthetic structural connectivity.

251   The simTB toolbox employs a data generation model that assumes spatiotemporal separability,

252   allowing the simulated fMRI data to be represented as the multiplication of spatial maps and time

253   courses. The generated data exhibit realistic dimensions, spatiotemporal activations, and noise

254   characteristics similar to those observed in typical fMRI datasets (Erhardt et al., 2012). Our fMRI

255   simulation consists of 16 ICNs for each of the 30 subjects, evenly divided into 3 distinct groups

256   (10 subjects per group) with varying design parameters (Group A, B and C). Generally, all spatial

257   maps have $V = 64 \times 64$ voxels (where V is the total number of voxels) and time courses are $T =$

258   3000 time points in length with a repetition time (TR) of 2 seconds. Spatial maps of the ICNs

259   represented in **Figure 2** correspond to the regions in the FiberCup data shown in **Figure 1**.

260   Groups A, B, and C differ in four ways, as outlined below. Firstly, the noise level for each group

261   was specifically selected to determine the robustness of the proposed model. For Group A, the

262   mean was 1.7, with a standard deviation of 0.2; for Group B, the mean was 1.5 with a standard

263   deviation of 0.4; and for Group C, the mean was 1.1 with a standard deviation of 0.35. Secondly,

264   to introduce diversity among the ICNs across different Groups, we implemented additional

265   adjustments to both the amplitudes (g_{ic}), and shapes of the reference ICNs. For ICN 6 in Group A,

266   we selected a weaker amplitude compared to Group B and C, while Group C had a weaker

267   amplitude for ICNs 8 and 11 compared to Groups A and B. The amplitudes of the ICNs (g_{ic}) were

268   modeled on a normal distribution. For instance, the distribution of ICN 6 (g_{ic6}) is normal with a

269   mean of 2.5 and a standard deviation of 0.3 for Group A, and a mean of 3.5 with a standard

270   deviation of 0.3 for Group B. Similarly, ICN 8 and 11 in Group C follow a normal distribution

271   with a mean of 2.5 and a standard deviation of 0.3, whereas Groups A and B have a mean of 3.5

272   and a standard deviation of 0.3. Additionally, each ICN underwent distinct transitions in the x and

273   y directions, as well as rotations, introducing unique changes. Moreover, the ICNs in Groups A

274   and C were expanded by factors of 1.2 and 1.3, respectively, while the ICNs in Group B were

275   contracted by a factor of 0.9.

276   Then, we constructed a synthetic ICN template to be used as a prior spatial map in the constrained

277   ICA model. The synthetic template was determined by averaging each ICN over all groups and

278   introducing deformation and noise.

279

280

281

282

283

284

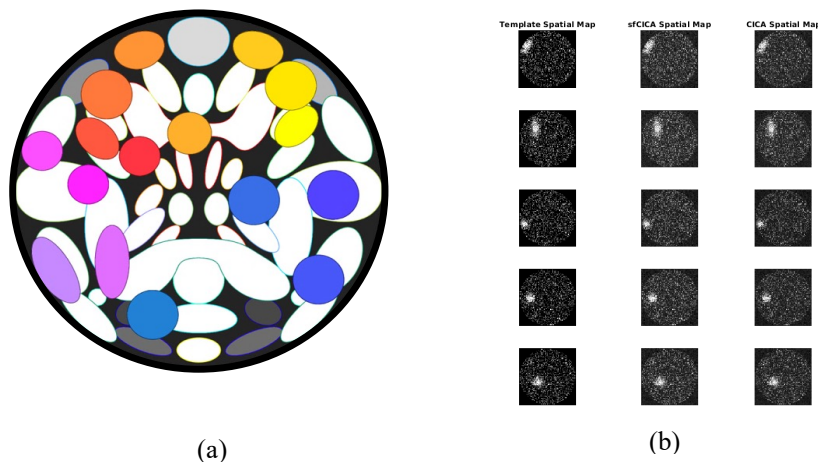(a)   (b)

Figure 2. (a) It represents the 16 spatial maps of the ICNs, derived from the FiberCup regions, inserted into the simTB toolbox as a reference to generate synthetic fMRI images. Using the generated synthetic data, we determined an average template, shown in the first column from the left (b), to be used as a prior spatial map. The second and third columns from the left in (b) illustrate examples of estimated ICNs by the sfCICA and CICA model using synthetic fMRI.

Evaluation criteria. Our model works on decreasing the weighted distance between time courses of the structurally connected ICNs. To ensure the objective is preserved, we used a distance metric and sparsity to measure the effect of the structural connectivity constraint on TCs. For this purpose, the sum of the distances between an ICN with all other ICs was determined utilizing the Euclidean distance as outlined in **Eq 9.**

$$\text{Dis} = \sum_{j=1}^{L} \left\| w_l - w_j \right\|^2 \tag{9}$$

where w_l is the time course of ICN number l and w_j is the time courses of all other remaining ICNs. This measure was estimated for both the sfCICA and CICA models.

Sparsity was measured as the number of weak connections to all possible connections in the FNC. To identify weak connections, we first determined an optimal threshold by maximizing the global cost-efficiency of the brain networks (Bassett et al., 2009), (here a threshold of 0.45 was

14

305 determined). The remaining connections after this threshold were considered strong connections

306 (ST). Then, all FNC networks were thresholded to retain strong connections and sparsity as

307 follows.

$$SP = \frac{N - ST}{N} \tag{10}$$

308 Where ST is the number of strong connections and N is the total number of possible connections.

309 Moreover, the robustness of the model was assessed by varying noise levels across the three

310 distinct simulated groups.

311 **2.2.2. Real data**

312 In this study, the real rs-fMRI and dMRI images were used from the Function Biomedical

313 Informatics Research Network (FBIRN) phase III datasets (Keator et al., 2016). Data collection

314 was at multiple sites of healthy control (HC) subjects or with schizophrenia (SZ) disorder. FBIRN

315 dataset consists of rs-fMRI and dMRI images from 311 age-gender-matched adults (age ranging

316 from 18 to 65 years old). It is 162 healthy controls (HC) including 115 male and 45 female (Avg

317 ± SD age: 37.0 ± 10.9) and 149 schizophrenia (SZ) patients including 115 male and 36 female

318 (Avg ± SD age: 38.7 ± 11.6).

319 **Acquisition.** Images were scanned at six 3T Siemens Tim Trio System and one 3T GE Discovery

320 MR750 scanner at multiple sites. The acquisition parameters of the rs-fMRI imaging were as

321 follows: FOV of 220 × 220 mm (64 × 64 matrix), TR = 2 s, TE = 30 ms, flip angle (FA) = 77°,

322 162 volumes, 32 sequential ascending axial slices of 4 mm thickness and 1 mm skip. Subjects had

323 their eyes closed during the resting state scan. For more details see (Keator et al., 2016). For the

324 dMRI images, scanning protocols were settled virtually to ensure equivalent acquisitions with 30

325 directions of diffusion gradient at b = 800 s/mm^2 and five measurements of b = 0 (b0) s/mm^2

326 (Keator et al., 2016).

327   **rs-fMRI preprocessing.** The rs-fMRI images were preprocessed via the statistical parametric

328   mapping (SPM12, http://www.fil.ion.ucl.ac.uk/spm/) toolbox in MATLAB 2020b, following the

329   procedure outlined in (Iraji, Fu, et al., 2022). The main steps of the preprocessing included

330   removing the first five fMRI timepoints, motion correction, slice timing correction, image

331   registering to the standard Montreal Neurological Institute (MNI) space, spatial resampling (to 3

332     $\times$ 3 $\times$3 mm^3 isotropic voxels), spatial smoothing using Gaussian kernel with a full width at half

333   maximum (FWHM) = 6 mm.

334   **dMRI preprocessing.** For preprocessing of the dMRI images, first, all images were corrected for

335   eddy current and motion distortions using the eddy package (FSL 6.0 (Jenkinson et al., 2012)) by

336   motion induced signal dropout detection based on b0 volumes and replacement method

337   (Andersson & Sotiropoulos, 2016). Then, a data quality check was performed by an in-house

338   developed algorithm and visual inspection to exclude images with extreme head motion, signal

339   dropout, or noise level (Caprihan et al., 2011; Wu et al., 2015).

340   An additional step was carried out on preprocessed dMRI images to determine white matter fiber

341   tracts for constructing structural connectivity. First, we used linear regression under the dtifit in

342   the FSL toolbox (Jenkinson et al., 2012) to model a voxel-wise diffusion tensor. The estimated

343   diffusion tensors were employed in deterministic tractography using the CAMINO toolbox (Cook

344   et al., 2006). This procedure involved three stopping criteria: a fixed step size of 0.5mm, an

345   anisotropy threshold of 0.2, and an angular threshold of 60° (Cook et al., 2006). All fiber tracts

346   were extracted in native space. Next, we transformed the native fractional anisotropy (FA) maps

347   into the standard MNI space using advanced normalizations tools (ANTs) (Avants et al., 2009).

348   Then we applied inverted spatial normalization to the Neuromark_fMRI_1.0 atlas (including N =

349   53 ICNs) (Du et al., 2020) to obtain the corresponding atlas in native space.

350   The ICNs of the normalized Neuromark_fMRI_1.0 atlas, which divides the brain into distinct

351   regions, were used as nodes in the network to build the structural connectivity network. For each

352   subject, we reconstructed an $N \times N$ structural connectivity network (M), counting the number of

353   streamlines connecting pairs of nodes.

354   **Evaluation criteria.** First, to determine the effect of the defined objective function in our

355   multimodal model, we used the same criteria adopted for the synthetic data. Consequently, for the

356   ICNs of each model (sfCICA and CICA), the distance was estimated using **Eq. 9**. Then, we

357   computed the sparsity of the estimated FNCs as in **Eq. 10**.

358   To enhance distance representation, we determined the difference of the measured distances, as

359   shown in **Eq. 11.**

$$Diff = \text{Dis}_{sfCICA} - \text{Dis}_{CICA} \tag{11}$$

360   In addition, we evaluated the proposed model with real data, using a set of statistical analysis. A

361   Paired t-test analysis was employed to determine if the examined ICNs from the sfCICA model,

362   constrained by structural connectivity, differ significantly from those of the CICA model. The

363   paired t-test analysis assesses whether the mean difference between paired observations is

364   significantly different from zero. Here, we used the time course of the ICNs and their FNC matrices

365   as observations for the paired t-test. FNC matrices were assessed using Pearson's correlation

366   among the time courses of the ICNs at the subject level for both the sfCICA and CICA models.

367   Moreover, for group comparison between subjects with schizophrenia (SZ) and healthy control

368   (HC), we applied a Generalized Linear Regression model (GLM) utilizing FNC matrices and

369   spatial maps. GLM analysis is a statistical technique that provides a flexible framework for

370   modeling the relationship between a dependent variable and one or more independent variables.

371   In this study, we used GLM to regress out effects of the age, sex, diagnosis, motion, and imaging

372   site effect as covariates for the FNC matrices and spatial maps. Additionally, false discovery rate

373   (FDR) correction was performed to adjust the estimated p-values.

374   Finally, to show that structural connectivity helps tune the FNCs we used network graph

375   parameters. To this end, graph theory analysis, utilizing FNC features was employed. We

376   estimated the FNCs as Pearson's correlation between TC related to each network (ICN) to

377   construct the FNC network at the individual level for both the CICA and sfCICA. Then, we

378   determined four common brain network parameters including modularity (Newman, 2006), local

379   and global efficiency (Latora & Marchiori, 2001), and small worldness (Amaral et al., 2000) to

380   characterize the graph properties of the resulting FNC. In addition, randomness (Vergara et al.,

381   2018), and sparsity were also examined.

382   In a brain network, modularity indicates the presence of functional modules involved in specific

383   cognitive processes (Newman, 2006). Local efficiency represents the efficiency of the

384   communications between regions (here ICNs) and global efficiency is the capacity of the network

385   for transferring information across the whole brain (Latora & Marchiori, 2001). Additionally,

386   small-worldness is the ratio of clustering to shortest path length, which summarizes the balance

387   between the efficiency and clustering in the brain network (Amaral et al., 2000).

388   **3. Results**

389   To determine multimodal ICNs through an iterative optimization, we applied the proposed sfCICA

390   model to the diffusion MRI (dMRI) and the resting-state fMRI (rs-fMRI) data obtained from 30

391   synthetic samples and 311 real subjects (146 HC and 162 SZ). The number of the ICNs was

392   determined based on a predefined standard ICN template, used as prior spatial maps. In this study,

393   the NeuroMark_1.0 template was utilized as prior maps for the real data. This template consists of

394   seven distinct functional domains, including subcortical (SC), sensorimotor (SM), auditory

395   (AUD), visual (VS), cognitive control (CC), default mode (DM), and cerebellum (CB). Our results

396   represent multimodal ICNs that are more informative and enhanced by incorporating multi-modal

397   information. They provide supporting evidence indicating the impact of the structural connectivity

398   information on neural activities (Litwińczuk et al., 2022).

399   **3.1. Estimated ICNs using synthetic datasets show a structural and functional learning**

400   **pattern.**

401   To determine the applicability and the robustness of the proposed model, we investigate the time

402   course distances of the ICNs, as a measure of the correlation, for both the sfCICA and the CICA

403   model at the subject level for different synthetic groups.

404   Distance analysis on the synthetic dataset predominantly revealed smaller distances after

405   performing structural connectivity constraints using the sfCICA model compared to the CICA

406   model, shown in **Figure 3.** This is reflected by average paired distances for the sfCICA (red box)

407   and the CICA (green box) model. **Figure 3,** column **(a)** displays average paired distances at the

408   subject level for each ICN. In all three groups of synthetic datasets, the average distances of the

409   sfCICA were primarily constrained by structural connectivity and decreased compared to the

410   CICA model. The corresponding group structural connectivity is shown in column **(b)**.

411   Statistical analysis, employing a paired t-test, revealed significant differences (p-value <0.05, FDR

412   correction: q< 0.05) in the average group distances between the sfCICA and the CICA model for

413   all the ICNs, except for ICN 14 in Group B, and ICN 1, 3, 7, 8, 11, 13, 14, 15 and, 16 in Group C.
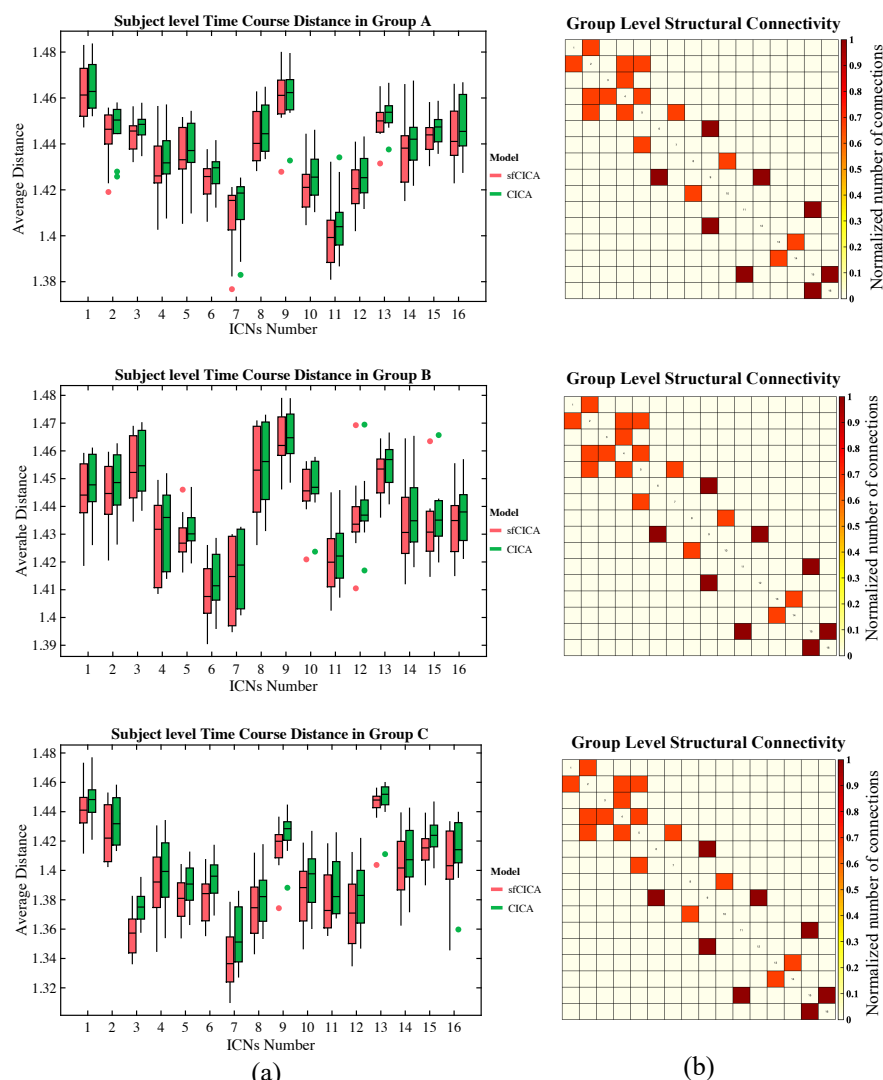
414

415

416

417

Figure 3. (**a**) Shows the average time course distance of the three groups of synthetic data, comparing the sfCICA (red box) to CICA (green box) at the subject level for each ICN. (**b**) Displays the corresponding group-level structural connectivity.

Figure 4. represents the time course distance of an ICN (here ICNs 2 and 15) from other connected ICNs at the subject level across three different groups using both the sfCICA and CICA models. We specifically selected ICNs with varying connection weights: one exhibiting a high structural connection (ICN number 2) and another with a low structural connection (ICN number 15) to other ICNs. The results in **Figure 4.** illustrate a greater decrease in time course distance for the connected ICNs in the sfCICA model (red box) compared to the CICA (green box). As expected, in the

445 subject-level analysis, the distance between ICNs in the sfCICA model decreased more

446 significantly than those in the CICA model.

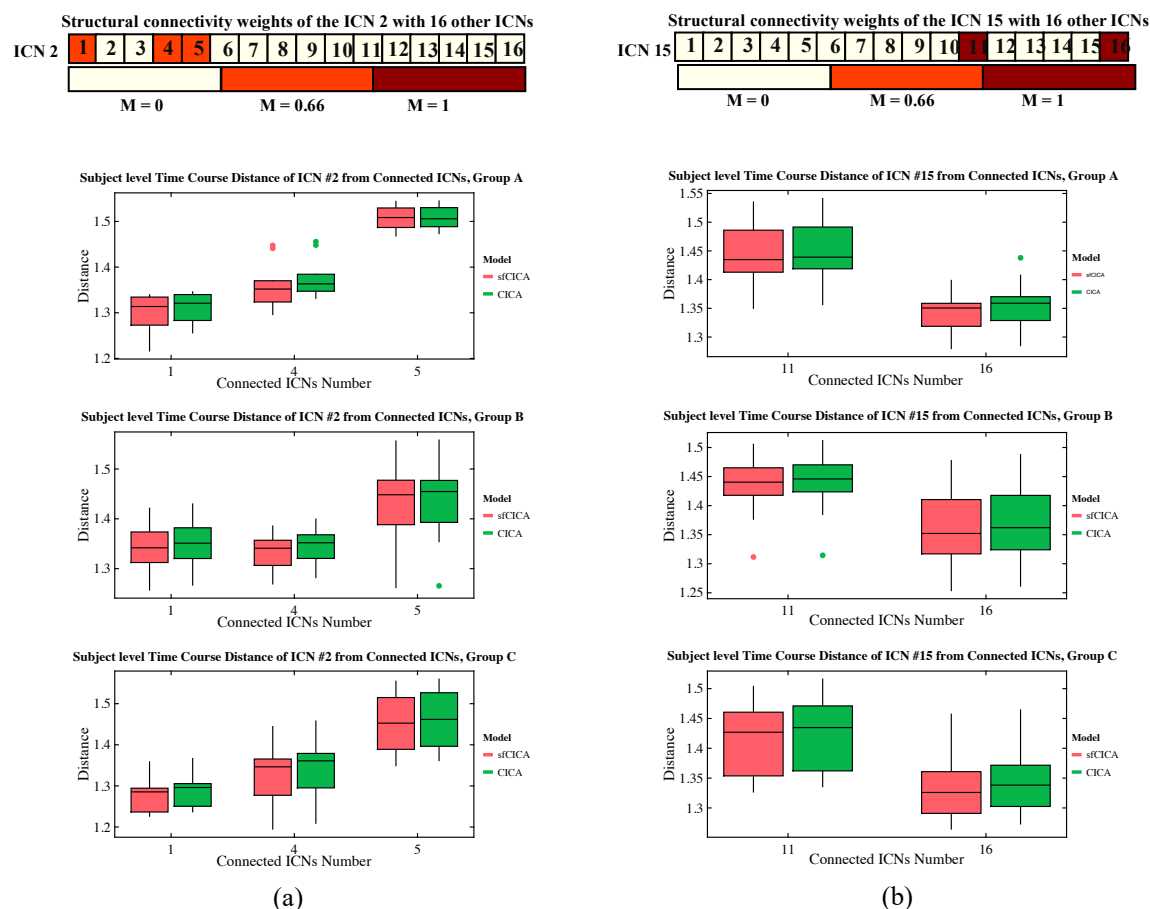(a)   (b)

Figure 4. It depicts the estimated time course distance of ICN 2 and 15 with other connected ICNs at the subject level, shown in columns (**a**) and (**b**) respectively. The time course distance of the ICNs in sfCICA model was lower compared to CICA. The corresponding structural connectivity of ICN 2 and 15 with other ICNs comes at top of each column (**a**) and (**b**).

466 Moreover, we examined changes in distance specifically between two pairs of ICNs: one with a

467 connection (between ICNs 2- 4) and another without a connection (between ICNs 2- 13), across

468 three different synthetic datasets in **Figure 5 (a-c)**. The time course distance between ICN 2 - 4

469 (with strong structural connectivity, M = 0.66) and ICN 2 -13 (without structural connectivity) was

470 investigated at the subject level. Results show that the proposed model exhibits a lower distance

471 compared to CICA for ICN 2-4 consistently across all subjects and various groups with different

472 noise levels. However, for ICNs 2 - 13 (without structural connectivity), the time course distance

473 for both sfCICA and CICA models was similar. The distance for the connected ICNs (e.g. 2-4) is

474 higher than that for the unconnected ICNs (e.g. 2-13) when comparing the distance results between

475 ICN 2- 4 and ICN 2- 13 at the subject level. The decrease in time course distance observed for

476 connected ICNs in the sfCICA model is greater than in the CICA model. This reflects the influence

477 of the structural connection and the adaptivity of our model in fluctuating the ICN estimation. For

478 the non-connected ICNs (without structural connectivity), only functional information was

479 effective, and the observed changes were consistently at a similar level for both models.
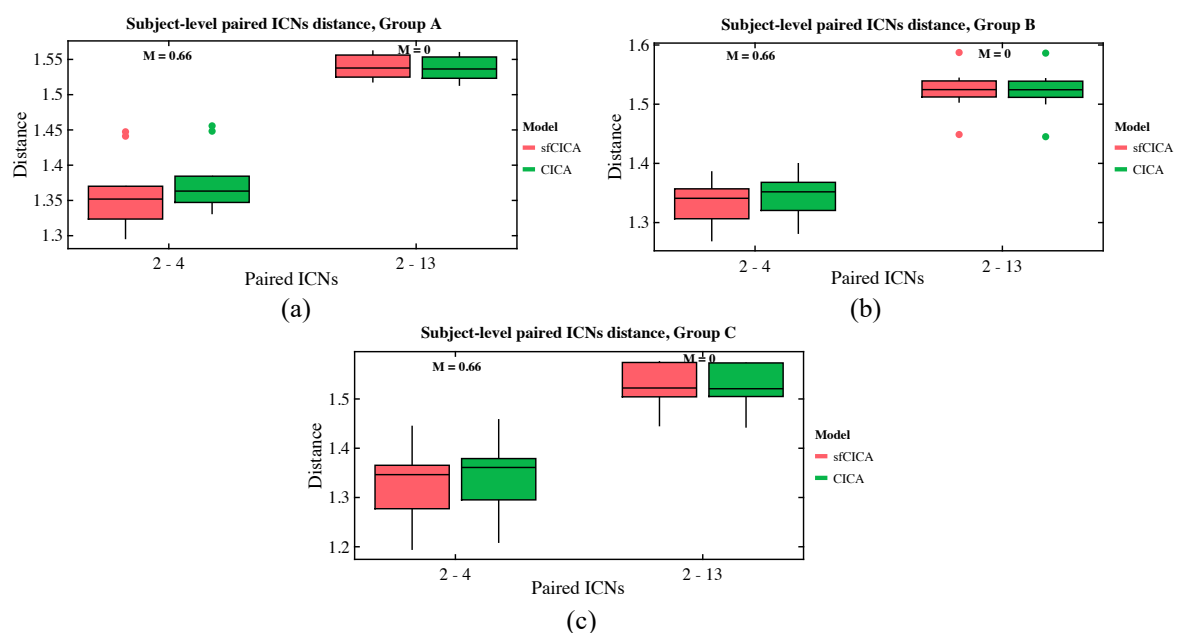
480

481

482

483

484 (a)

485

486

487

488 (c)

489 **Figure 5.** The time course distance of ICN 2 with a connected ICN (e.g 4) and a non-connected ICN (e.g. 13) is represented

490 for synthetic data with three different noise levels **(a-c)**. The distance decreased for connected ICNs (e.g. ICN 2- 4), while

491 the disconnected ICNs had similar distances across all subjects.

492

493 Statistical analysis using a two-sample t-test reveals an increase in various graph metrics,

494 (modularity: 0.352±0.01, global efficiency: 0.157±0.01, local efficiency: 0.199±0.009, small-

495 worldness: 1.415±0.055, non-randomness: 5.0±1.15) for sfCICA compared to CICA (modularity:

496 0.351±0.01, global efficiency: 0.155±0.01, local efficiency: 0.198±0.009, small-worldness:

497 1.412±0.006, non-randomness: 4.18±1.15). A slight, but insignificant decrease (p-value>0.05) was

498 observed between the sparsity measurements of the CICA (Mean±Std: 0.28±0.01) and sfCICA

499 (Mean±Std: 0.27±0.01) models.

3.2. FNC is informed by structural connectivity weights in synthetic data.

501 To emphasize the influence of the structural connectivity information on the FNC of ICNs in

502 synthetic data, we assess the similarity of the FNC with structural connectivity, as well as the

503 residual FNC for both the proposed sfCICA and the CICA models. The residual FNC is determined

504 as the difference between the FNC matrices from the sfCICA and CICA models (FNC_{diff} =

505 FNC_{sfCICA} - FNC_{CICA}).

506 We perform two different evaluations by computing the similarity of the FNC matrix to determine

507 the degree to which the structural connectivity impacted the resulting model weights, as shown in

508 **Figure. 6**. For this purpose, the FNC matrix of the estimated ICNs from the sfCICA model was

509 determined by computing Pearson's correlation between paired ICNs for each subject. The

510 similarity of the FNCs was then computed: (1) with structural connectivity and, (2) with FNC_{diff},

511 at the subject level. A similar procedure was performed on the ICNs from the CICA model, and

512 the results from both the sfCICA and CICA models were compared. From both evaluations,

513 FNC_{sfCICA} demonstrated higher similarity with FNC_{diff} and structural connectivity than FNC_{CICA}.

514 These results suggest that the proposed sfCICA model is informed by structural information and

515 remains robust to noise. Even with an increase in the noise level from Group A to C, the proposed

516   model showed improvement compared to the CICA model. However, FNC_{sfCICA} and FNC_{CICA}

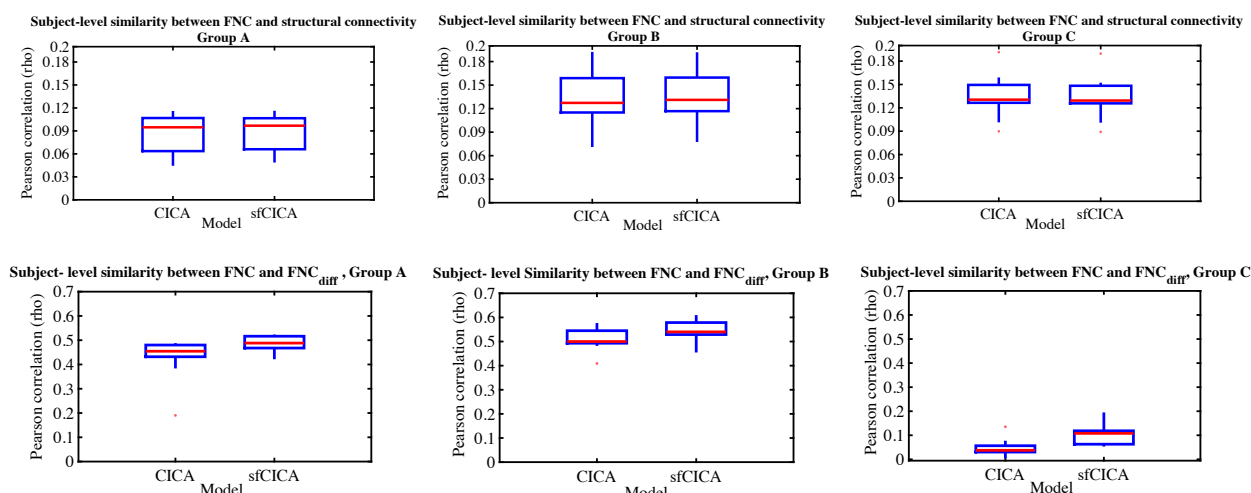517   exhibited the same level of similarity with structural connectivity.

518

Figure 6. Similarity (Pearson correlation) of the FNC matrix with structural connectivity and with FNC_{diff} (FNC_{diff} = FNC_{sfCICA} - FNC_{CICA}) was estimated for both the sfCICA and the CICA model across three distinct groups of synthetic data (columns). The results indicate that the sfCICA model exhibits a higher correlation with both structural connectivity and FNC_{diff} compared to CICA, as expected. Notably, greater differences were observed for FC_{diff}. Furthermore, the findings demonstrate the robustness of the proposed model to noise, as evidenced by its consistent performance even as noise increases from Group A to C.

3.3. The subject-level structural-functional ICNs show more modular and integrated networks for the FBIRN data.

533   Using the sfCICA model, the ICNs are guided by structural connectivity and FNC for each subject.

534   In this paper, we used the NeuroMark template (Du et al., 2020) as prior spatial information, and

535   the included information was evaluated by estimating the spatial similarity between the estimated

536   ICNs and the corresponding NeuroMark template networks using Pearson's correlation for both

537   the sfCICA and the CICA models. To analyze the effectiveness of the proposed model for both

538   healthy (HC) and disease (SZ) cases, we presented separate results for each group. In **Figure 7a,**

24

539   the results showed an unimodal Gaussian distribution for HC and a bimodal Gaussian-like

540   distribution in SZ, which is more clearly highlighted in the proposed model compared to the CICA

541   model. It illustrates more significant spatial similarity for all subjects in the sfCICA model (Mean:

542   0.52) compared to the CICA model (Mean: 0.47) across both HC and SZ cohorts from the FBIRN

543   dataset. On average, the sfCICA model exhibited a 10% increase in similarity compared to the

544   spatial similarity estimated by the CICA model. The enhanced spatial similarity observed with

545   standard and reproducible templates across multiple subjects suggests that informing the

546   optimization process using structural connectivity could improve the results.

547   Moreover, in **Figure 7b**, we computed and depicted the time course distance between paired ICNs

548   at the subject level to assess the impact of structural connectivity. As we expected, the estimated

549   distance showed a dependence on the structural connectivity weights, being consistently smaller

550   for all the ICNs estimated by sfCICA in comparison to the CICA model. Overall, the distances, as

551   well as the average distance of the time courses, were smaller in sfCICA than in CICA for both

552   HC and SZ subjects, indicating greater functional integration (paired t-test: p-value<0.05).

553   However, the increased spatial similarity resulted in more modular networks compared to the

554   CICA model. In this context, distance refers to the mean square distances between paired time

555   courses.
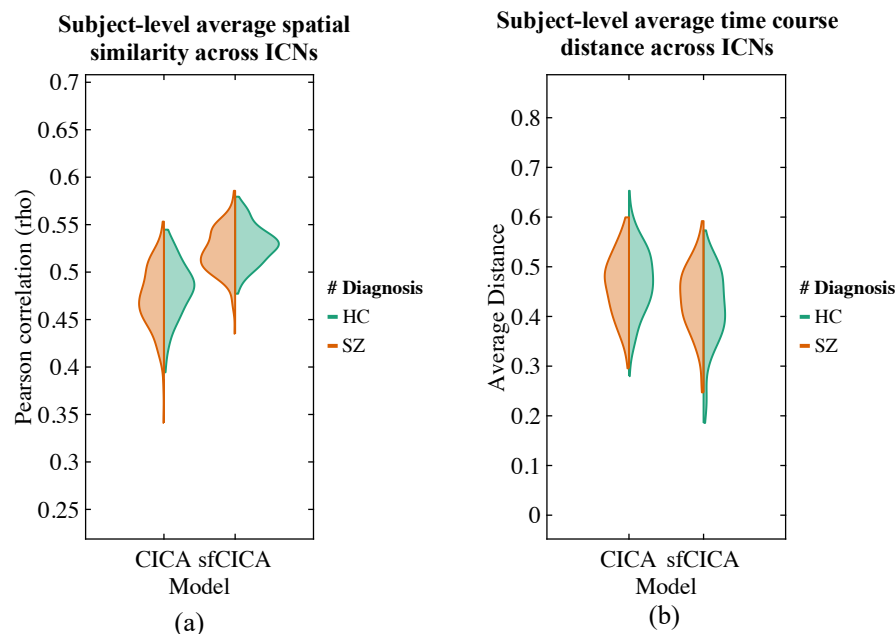
556

557

558

559

560

561

Figure 7. Distribution of average spatial similarity and time course distance over the ICNs at the subject level were represented for each model using FBIRN data. In (a), the distribution of the spatial similarity (Pearson correlation) with NeuroMark_01 template, used for prior spatial information, is illustrated for both the CICA and the sfCICA models in two groups: HC in green and SZ in red. Mean square distances of each time course from remaining time courses are shown in (b) within each HC (green) and SZ (red) group using the sfCICA and the CICA models. The sfCICA model showed higher spatial similarity and reduced time course distances.

3.4. The subject-level structural-functional ICNs show a structural and functional learning pattern for the FBIRN data.

Figure. 8 illustrates the differences in the estimated time course distances (a measure of the correlation) between the sfCICA and the CICA model for each ICN at the subject level. Negative distance values (below the pink line) indicate lower distances among ICNs in the sfCICA model compared to CICA. Interestingly, we observed predominantly negative correlations in the FBIRN dataset. In addition, ICN 18, 29, 37, 40, 4, 47, 48, 51, 52, and 53 show, on average, positive differences across all subjects. In general, we expect that ICNs with weak mean structural

596   connectivity weight (as shown in **Figure. 8**) will show higher distances in the sfCICA model than

597   in the CICA model, resulting in a positive average pattern for distance differences. **Figure. 8**

598   reveals that the weights of the structural connectivity are associated with the distance of the time

599   courses, i.e., where the structural connectivity is weak, the distance is large, and where the

600   structural connectivity is strong, the distance is small among the sfCICA relative to the CICA time

601   courses. These results suggest that both structural weights and functional spatial maps contribute

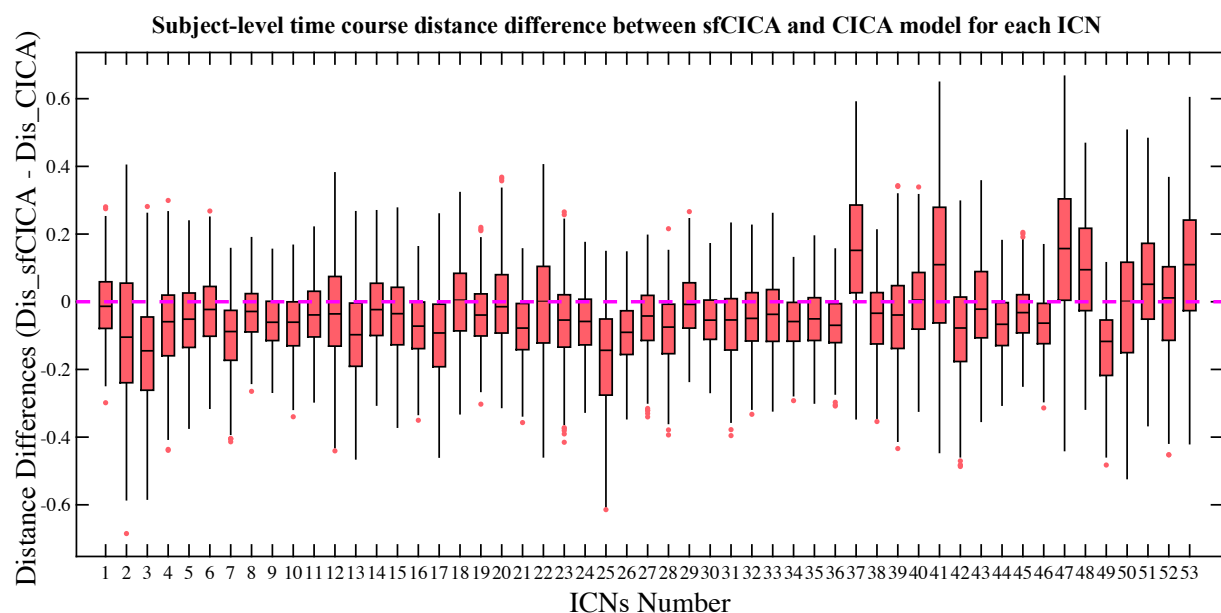602   complementary information to the estimated ICNs.

603

Figure 8. Illustrates that the differences in time course distances for most of the Intrinsic Connectivity Networks (ICNs) estimated by the sfCICA model, as compared to the CICA model in the FBIRN dataset, are smaller. The average distance differences of the time courses are predominantly negative, signifying smaller distances in the sfCICA compared to the CICA model, and this difference is influenced by Structural Connectivity.

617   We also estimated the time course distance for six randomly selected paired ICNs including 13-

618   22, 48-47, 13-52, 12-48, 2-37, and 3-5, with different structural connectivity weights from weak

619   to strong in the FBIRN data. As depicted in **Figure 9**, and similarly to the synthetic dataset, we

27

620   observed distinct time course distances between sfCICA and CICA, with a decrease in sfCICA as

621   the structural connectivity weights increased. On average over all subjects, our model (red box)

622   has a higher distance for ICN 13 with 22 and 52 (both weak structural connections) compared to

623   the CICA model (green box). For ICN 48, we consider two moderate (structural connectivity

624   weight, M = 0.2) and weak connections (0.002) respectively with ICN 12 and 47. Interestingly,

625   the distance between ICN 48 and 47 was increased compared to the CICA model, similar to the

626   distance between ICN 13 and 52 (structural connectivity weight, M = 0.037). Conversely, the

627   distance between ICN 48 and 12 was lower in our model. We evaluated the distance for the ICNs

628   with strong structural connection, ICN 37 with 2 (M = 0.66) and ICN 3 with 5 (M = 0.91). As

629   expected, for both connections, the distance decreased compared to the CICA model.
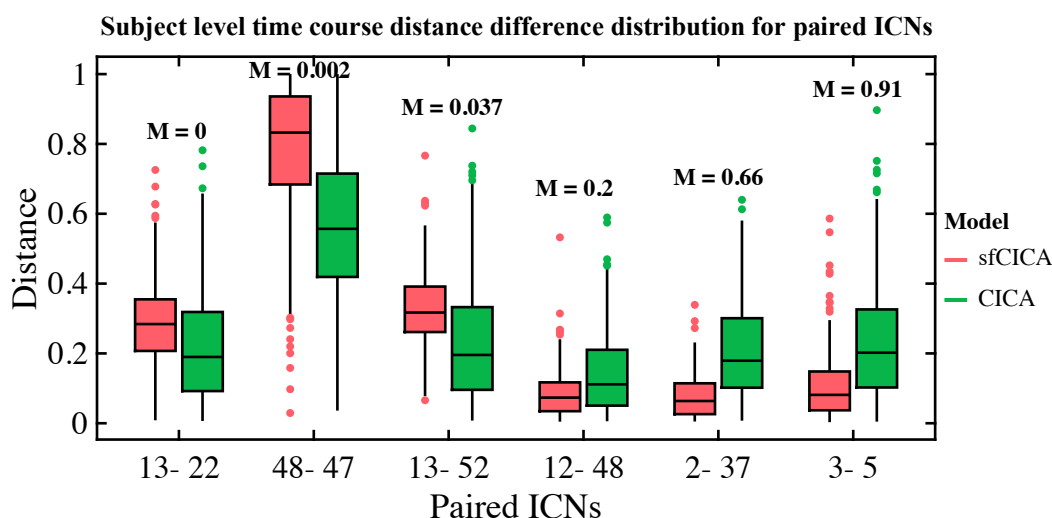
630

Figure 9. Depicts the distribution of time course distances for six paired ICNs estimated by both sfCICA and CICA models in the FBIRN dataset. These, paired ICNs were selected with varying structural connectivity weights ranging from weak to strong (0 - 0.91) connections. The estimated distance demonstrates an increase in structural connectivity weights, resulting in a decreased time course distance for the sfCICA model (red box) compared to the CICA model (green box). This highlights the influence of structural connectivity on the estimated ICNs.

3.5. Distinguished spatial patterns for the ICNs in the sfCICA compared to the CICA model

using the FBIRN data.

Significantly, we observed enhanced modularity and well-defined spatial maps in certain

functional networks represented by ICNs IC 2, 22, 42, 7, 11, 21, 13,14, 34, 37, 50, 3, 27, 39, and

42, across most subjects, especially in those diagnosed with schizophrenia. These observations

indicate that the structural connectivity constraints assist in better distinguishing between healthy

and patient subjects within these specific ICNs. These functional networks mostly include

subcortical, sensory networks (sensorimotor and, visual), default mode, and the cerebellum. In

Figure 10, three different ICNs for subjects 29, 30, 37, and 74 are depicted in each row. All ICNs

were converted to z-scores and thresholded at z-score>3, p-value<0.05. Additionally, a qualitative

examination reveals more modular networks compared to the CICA model, **(**refer to **Figure 11).**

Moreover, we performed paired t-test analysis between sfCICA and CICA using the spatial maps

within each group (HC / SZ) separately. In healthy subjects, significant differences (p-value<0.05)

were observed in most of the ICNs, except for the ICNs 45 and 51. ICNs 9, 27, and 51 in

schizophrenia showed no significant differences between sfCICA and CICA.

In addition, we computed graph-based network features such as modularity and randomness.

Utilizing FNC matrices derived from the estimated Intrinsic Connectivity Networks (ICNs), our

analysis revealed that the modularity coefficient for ICNs estimated with the sfCICA model was

statistically significant (paired t-test: p-value < 0.05, Mean±std = 0.24±0.03) compared to the

CICA model (Mean±std = 0.21±0.02). A randomness analysis was also conducted, indicating

significant differences in non-randomness. Specifically, the sfCICA model exhibited a lower

randomness coefficient (i.e., higher non-randomness characteristic) in the FNC patterns (paired t-

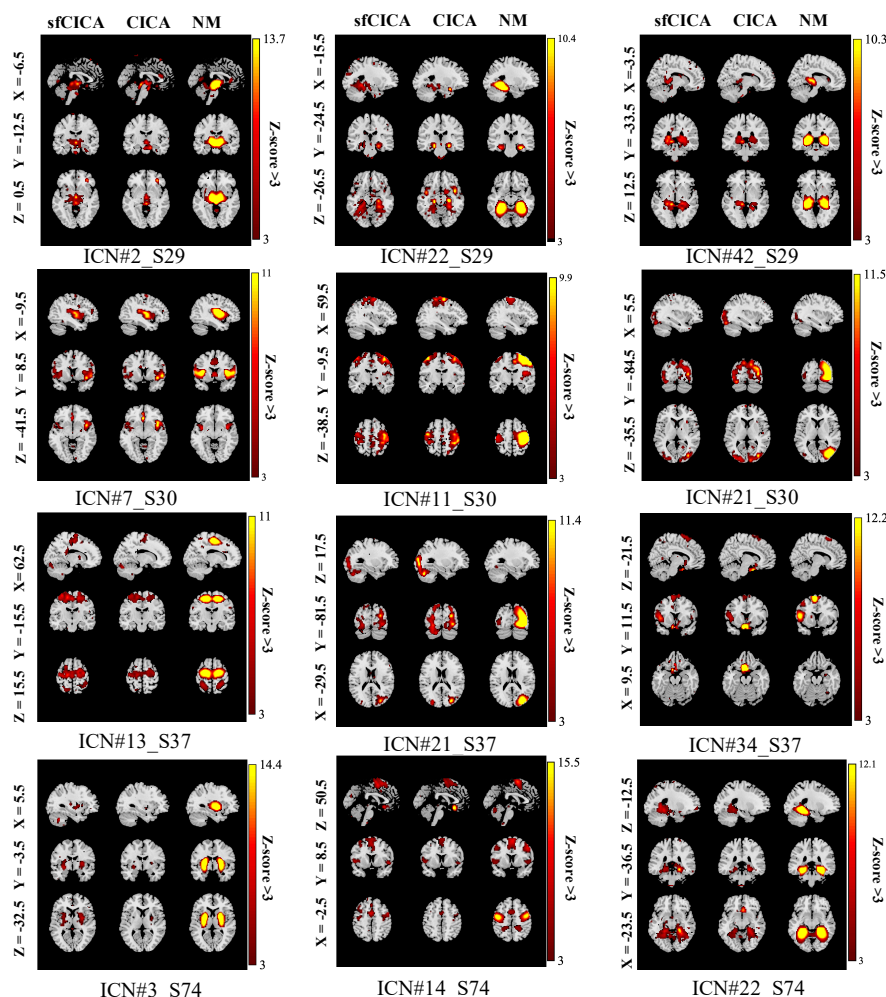test: p-value < 0.05, Mean±std = 13.3±3.5) compared to the CICA model (Mean±std = 11.5±2.05).

29

Figure 10. Each column displays spatial maps for selected ICNs (z-score>3) derived from different subjects using sfCICA, CICA, and the NeuroMark template (NM). The sfCICA consistently exhibits more modular characteristics (average modularity for sfCICA: 0.24, for the CICA: 0.21) across different subjects compared to the CICA model.

3.6. FNC of the Structural-functional connectivity informed ICNs revealed significantly constrained/ learned from structural connectivity using the FBIRN data.

To determine the differences between the CICA and sfCICA models, we applied a paired t-test analysis on FNC matrices. Interestingly the paired t-tests indicated rejection of the null hypothesis, signifying significant differences between sfCICA and CICA across all ICNs. The estimated t-

691   values (**Figure. 11a**) represented significant differences in ICNs related to the SC, SM, VS, CC,

692   and DM networks. Paired t-test analysis was also performed regarding the absolute value for the

693   FNCs, as illustrated in **Figure. 11b,** it shows reduced t-values for certain ICNs within the AUD,

694   SM, VS, CC, DM, and CB networks. It replicates a decrease in the FNC association between the

695   two models and can be explained based on the hypothesis that the impact of the relationship

696   between structural connectivity and FNC on cognitive performance may depend on the functional

697   domain.

698   Moreover, regarding **Figure. 11 (a-d)**, and the comparison of structural connectivity patterns

699   (**Figure 11(c-d)**) with paired t-test analysis (**Figure 11(a-b)**), it is apparent that the structural

700   connectivity weights optimize the distances, thereby enhancing the estimation of the ICNs.

701   Further, analysis of the paired t-test between ICNs of both models reveals similarity for ICNs 1,

702   6, 11, 12, 14, 15, 18, 20, 22, 29, 39, 40, 43, 45, 50, and 52.

703

704

705
706
707
708
709
710
711
712
713
714
715
716
717
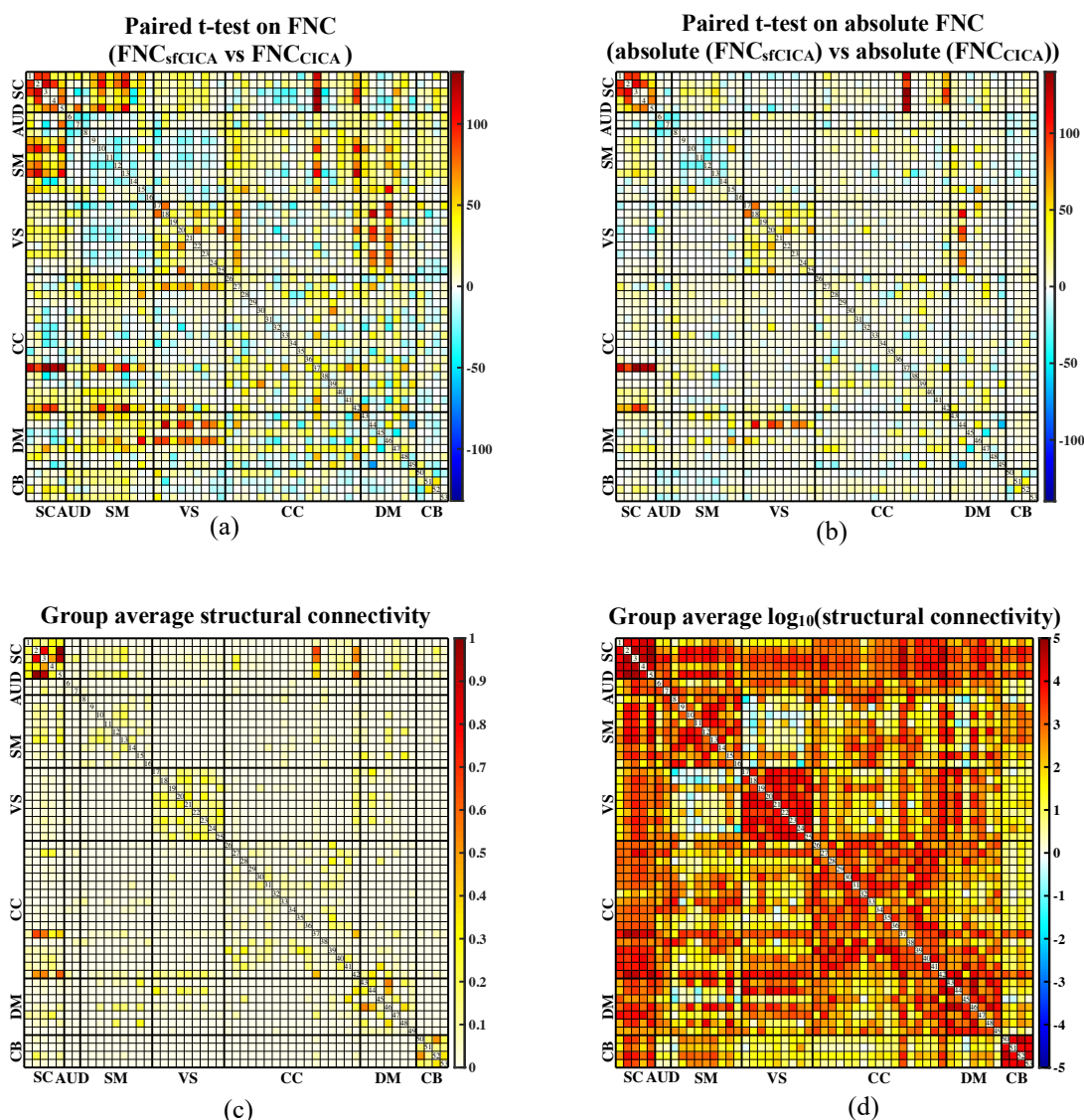718
719
720
721
722
723
724
725
726

Figure 11. Illustrates the results for the paired t-test analysis between the FNC matrices of the sfCICA and CICA models, along with their corresponding structural connectivity, using FBIRN dataset. FNC represents the Pearson correlation between the estimated ICNs of each model. In (**a**). T-value maps for the paired t-test using FNC are shown, while (**b**) displays the t-map for the absolute FNCs. sfCICA model exhibits higher values in most ICNs compared to the CICA model. The group average structural connectivity, and its logarithmic scale connection weights ($log_{10}(connection\ weights)$), are represented in (**b**) and (**c**). The weights of the structural connectivity indicate the number of tracts connecting two ICNs.

775　The determined results were jointly estimated by incorporating information from the structural

776　connectivity weights into the correlation between the time courses overall time (i.e., the FNC

777　matrix). A similar analysis on synthetic data was conducted on real data as well to assess the

778　similarity of the FNC with structural connectivity and FNC with FNC_{diff}, determining the extent

779　to which structural connectivity impacts the resulting model weights, as illustrated in **Figure. 12**.

780　For this purpose, an FNC matrix was computed for each subject using Pearson's correlation among

781　the time courses of the ICNs determined by the sfCICA model. A similar procedure was performed

782　to estimate FNC_{CICA} using the ICNs of the CICA model. The comparison of results from both the

783　sfCICA and CICA models indicated that in real datasets (FBIRN), FNC_{sfCICA} exhibits greater

784　similarity with structural connectivity and FNC_{diff} to FNC_{CICA}. It indicates the proposed sfCICA

785　model is informed by structural information, showing the multi-modal sfCICA model provides

786　additional information that could capture variability between subjects and between groups.

787

(a)　(b)
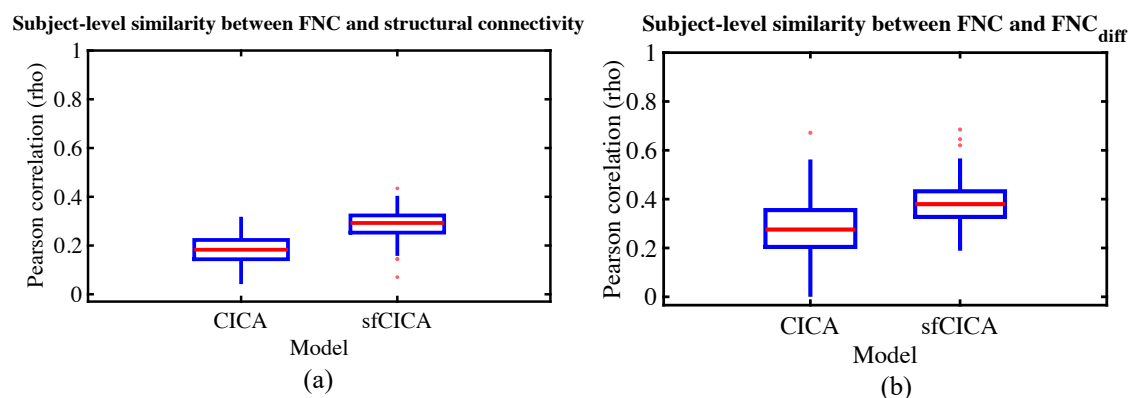
799　**Figure 12.** Similarity (Pearson correlation) between FNC matrix of estimated ICNs from the sfCICA model with

800　structural connectivity and, residual (diff) FNC matrix is represented for FBIRN dataset respectively in (**a**) and (**b**).

801　Results show similarity (correlation) with both structural connectivity and residual FNC (FNC_{diff}) is higher for the

802　sfCICA model than the CICA, representing more informatic ICNs.

803

3.7. Structural-functional connectivity-informed ICNs reveal significant differences between controls and schizophrenia subjects using the FBIRN data.

Figure. 13 (**a-b**) show the average FNC across all subjects for the sfCICA and CICA models. Additionally, group differences analysis using FNC for the HC vs SZ was performed and the results are represented in **Figure. 13 (c-d).**

Furthermore, to investigate the ability of the proposed method to find group differences (healthy/ patient) in FNC patterns using both the sfCICA and the CICA models, a generalized linear regression model (GLM) was performed with multiple covariates (**Figure. 13** (**c-d**)). The results indicated a more significant correlation (p-value<0.05, FDR: q<0.03) across all networks (displayed with red stars) comparing HC vs SZ group for the sfCICA model. We detected 503 significant cells in the upper triangle for the sfCICA model (**Figure 13 c**), a notable increase compared to the 421 significant cells observed for the CICA model (**Figure 13 d**). Correlations of the sensory networks were less significant in the sfCICA model compared to the CICA. In contrast, SC-related regions showed more significance. The findings suggested the involvement of structural connectivity in the SC domain, a factor not observed with the CICA model. ICNs for the SC, DMN, and CB networks exhibited significantly higher FNC in HC compared to SZ for the sfCICA model (**Figure. 13 c**), while sensory-related networks (AUD, VS, and SM) and CC network showed significantly higher FNC in HC compared to SZ for both models (**Figure. 13 (c-d)**). This suggests that considering structural connectivity plays an important role in identifying the FNC of the SC and that the sfCICA which jointly analyzes structural and functional ICA output provides a more sensitive model. The values illustrated in the higher triangle of matrices in **Figure 13 (c-d)**, are -log10(p_value) $\times$ $sign$ (t_value) and t-values are represented in the lower triangle.
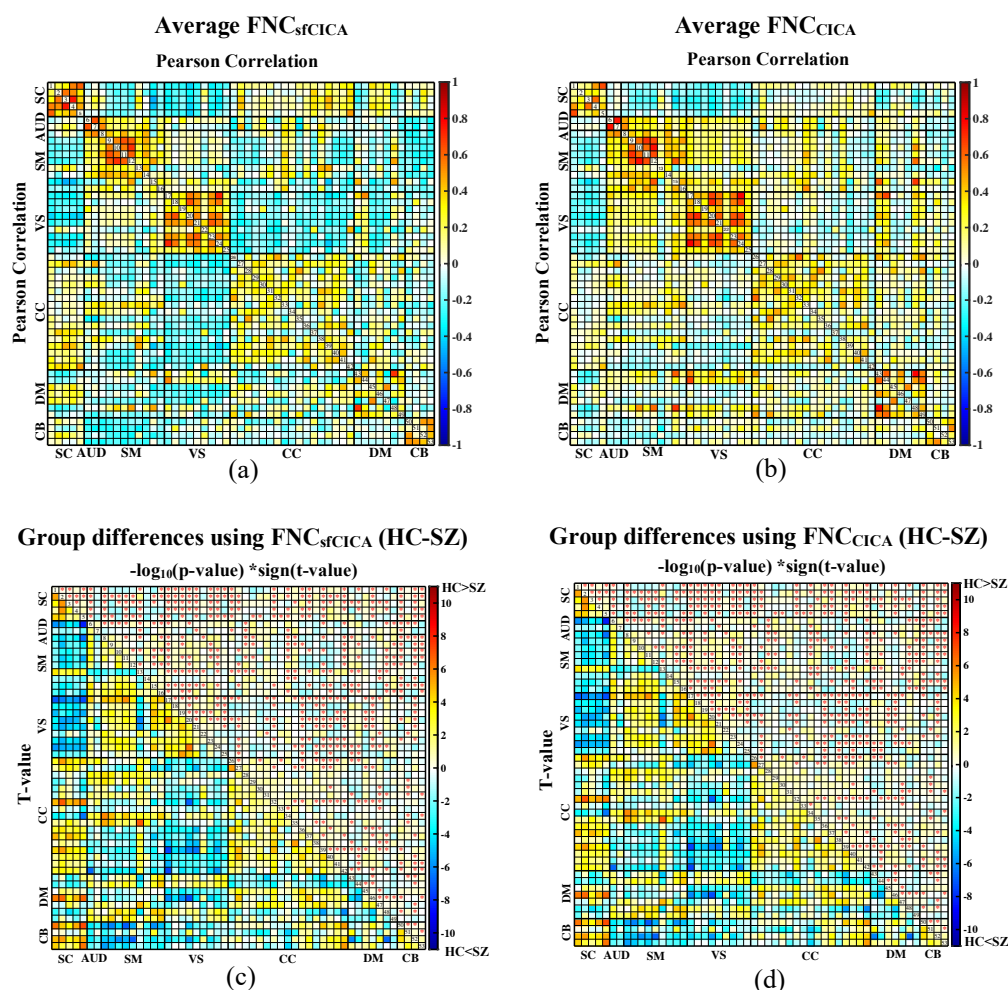
Figure 13. Average FNC estimated across all subjects and statistical group difference maps (HC/ SZ) for the FBIRN dataset. In **(a)** and **(b),** the average FNC of all subjects is presented for the sfCICA and CICA models respectively. For the group (HC/ SZ) difference comparison, GLM analysis was performed to regress out covariates including age, sex, motion, imaging site, and diagnosis from the FNC matrices. More significant differences (p-value<0.05 and FDR<0.03), represented by red stars, were observed between HC and SZ in the proposed sfCICA compared to the CICA model. Results were corrected for multiple comparisons using false discovery rate (FDR) with q<0.03; and represented in **(c-d)**, which upper triangle each cell of the matrices are *-log₁₀(p-value) *sign(t-value)* and lower triangle is t-value. ICNs were categorized in seven different domains including subcortical network (SC), auditory network (AUD), sensorimotor network (SM), visual network (VS), cognitive control network (CC), default mode network (DM) and cerebellum (CB). Results show that FNC in HC are higher than SZ in most of the ICNs, in the sfCICA compared to the CICA model.

35

877 **3.8. Multimodal ICNs represent more significant spatial maps between groups (controls**

878 **and schizophrenia) using the FBIRN data.**

879 To investigate the hypothesis of the proposed model, we conducted a group differences analysis

880 between HC and SZ on the ICN spatial maps. For this purpose, a GLM analysis was adopted to

881 regress out the effect of age, sex, motion, site, and diagnosis per ICN. Table 1 displays the

882 percentage of significant voxels in each ICN of different networks. Results indicate that out of

883 fifty-three ICNs, thirty-two showed a higher number of significant voxels (p-value<0.05) in the

884 sfCICA model (dark blue rows). Conversely, in the remaining twenty-one ICNs, five (light blue

885 row) demonstrated a similar percentage of significant voxels, and sixteens (white rows)

886 represented a lower percentage with a deviation for the sfCICA model.

887 In addition, network properties including modularity, efficiency, small-worldness, randomness,

888 and sparsity were estimated using FNC features. Results (Table 2) showed significantly higher (p-

889 value<0.05) efficiency, modularity, and randomness for the sfCICA model using the FNC feature.

890 Small-worldness was also greater for sfCICA but the difference between the two models was not

891 significant.

892

893

894

895

896

897

898 **Table 1.** Shows the percentage of the significant voxels in each ICN using group differences analysis. ICNs (rows)

899 with higher values for the sfCICA are represented in dark blue, while light blue and white indicate equal or lower

900 values for the sfCICA compared to the CICA.

Networks	ICNs	Number of significant voxels using CICA (%)	Number of significant voxels using sfCICA (%)	Differences between significant voxels, sfCICA – CICA (%)
SC	IC1	4.9	5.6	0.7
	IC2	4.1	6	1.9
	IC3	4.2	4.9	0.7
	IC4	3	3.5	0.5
	IC5	8.3	9.6	1.3
AUD	IC1	2.8	2.9	0.1
	IC2	4.7	5.4	0.7
SM	IC1	2.1	2.9	0.7
	IC2	2.8	3.4	0.6
	IC3	7.1	5.7	-1.4
	IC4	8.3	9.1	0.8
	IC5	5.5	5.8	0.3
	IC6	4.4	4.2	-0.2
	IC7	3.9	3.9	0
	IC8	6.6	7	0.4
	IC9	5	5.1	0.1
VS	IC1	3.2	4.1	0.9
	IC2	10	10	0
	IC3	5.1	5.2	0.1
	IC4	8	6.8	-1.2
	IC5	3.5	4.2	0.7
	IC6	3.1	3.4	0.3
	IC7	3.8	4.5	0.7
	IC8	2.4	2.4	0
	IC9	4.1	4.8	0.7
CC	IC1	5.1	5.1	0
	IC2	8.2	7.3	-0.9
	IC3	5.5	5.9	0.4
	IC4	5.3	5.2	-0.1
	IC5	6.6	6.7	0.1
	IC6	6.7	6.2	-0.5
	IC7	5.2	6	0.8
	IC8	8.9	6.3	-2.6
	IC9	8	8.3	0.3
	IC10	7	6.4	-0.6
	IC11	9.2	8	-0.8
	IC12	3.3	3.7	0.4
	IC13	8	8.3	0.3
	IC14	4.3	5.5	1.2
	IC15	7	5.4	-1.6
	IC16	4.2	4.2	0
	IC17	5.6	5.3	-0.3
DM	IC1	3.1	3.4	0.3
	IC2	3.5	3.2	-0.3
	IC3	2.5	3.2	0.7
	IC4	8.2	8.1	-0.1
	IC5	4.5	3.6	-0.9
	IC6	5.1	5.2	0.1
	IC7	7.6	6	-1.6
CB	IC1	2.1	4.8	2.7
	IC2	9.1	6.4	-2.7
	IC3	2.1	5.9	3.8
	IC4	4.6	5.6	1

901

902

903
Table 2. Graph parameters estimated for the FNC matrices.

Graph parameters	Single-modality Model (**Mean±std**)	Multi-modality Model (**Mean±std**)
Modularity	**0.21±0.02**	**0.24±0.03**
Local efficiency	**0.32±0.01**	**0.37±0.01**
Global efficiency	**0.30±0.03**	**0.33±0.03**
Small-worldness	**1.15±0.08**	**1.17±0.06**
Non- Randomness	**11.30±3.50**	**13.50±2.05**
Sparsity	**0.28±0.01**	**0.27±0.01**

904

905   **4. Discussion**

906   This study proposes a new, joint structural-functional, data-driven model to estimate intrinsic

907   functional connectivity networks (ICNs) using multi-modal brain images. While most of the

908   studies typically rely on fixed regions weighted by diffusion MRI (dMRI), our proposed approach

909   is a multi-modal ICA model, named sfCICA, which is guided by the structural and functional

910   connectivity network domain. Using network science, structural and functional information is

911   compressed in nodes and edges which has become a common practice in neuroscience to

912   understand functional interactions in the brain (Babaeeghazvini et al., 2021). In the sfCICA model,

913   the functional connectivity from resting-state magnetic resonance imaging is constrained by

914   structural connectivity weights (normalized number of streams). We applied the proposed model

915   to datasets from subjects with schizophrenia and healthy controls, as well as simulated data.

916   Through this new model, we identified improved spatial maps, individual subject variability, and

917   modularity of the FNC networks. Furthermore, the sfCICA model exhibits less randomness and

38

918   greater sensitivity to group differences in healthy controls and subjects with schizophrenia (HC/SZ

919   subjects).

920   Most previous ICA models are focused on functional information or functional information with

921   prior spatial constraints (Du & Fan, 2013; Du et al., 2020). In recent years, there has been a shift

922   towards multi-modal models, incorporating features estimated from different modalities through

923   joint analysis (Wu & Calhoun, 2023). Joint-ICA, parallel ICA, link-ICA, and cmICA models

924   utilize features from fMRI, dMRI, or sMRI, such as connectivity, fractional anisotropy, and

925   structural measures to identify functional networks. The proposed model in this study diverges by

926   simultaneously learning from both functional and structural connectivity. This approach aims to

927   constrain functional changes over time based on estimates of structural connectivity.

928   Less work has been given to dMRI connectivity, as in the cmICA model (Wu & Calhoun, 2023).

929   cmICA (Wu & Calhoun, 2023), uses multi-modal fMRI and dMRI, integrating features derived

930   from each modality to identify ICNs shared between structural connectivity and FNC,

931   acknowledging that there might be a mismatch between features from each modality. Although

932   cmICA attempts to address this, the contributions of features from each modality are asymmetrical

933   (Wu & Calhoun, 2023). In contrast, our proposed model is based on both direct and indirect

934   features and the contribution of each modality enhances the other. Thus, when structural

935   connectivity weights are strong, functional data exhibits a higher correlation, while weaker

936   structural connectivity weights result in less correlated functional data. Notably, the sfCICA model

937   relies on two main concepts of an ICA analysis, maximizing independence and similarity, and tries

938   to estimate intrinsic brain functional networks which are optimized based on both structural and

939   functional connectivity information. Therefore, we posit that the proposed joint multi-modal

940   information integration allows for better characterization of healthy and disordered brain

941   connectivity (Iraji et al., 2016; Wu & Calhoun, 2023). Characterization of the intrinsic brain

942   activity, known as functional network modeling, has been widely used in human brain studies,

943   particularly because of its relevance to brain disorder research (Wang et al., 2021). One of the

944   greatest advancements in this area was uncovered by rs-fMRI images using ICA analysis (Calhoun

945   et al., 2001) and continues to advance for the field by the inclusion of additional imaging

946   modalities.

947   Including two different modalities of information in our model, the replicability and noise

948   robustness of the proposed model were assessed through three different synthetic datasets (**Figures**

949   **3, 4, and 5**). Each group has different levels of signal-to-noise ratio (SNR), and for each group, a

950   similar pattern, constrained by structural connectivity, was observed. Our findings highlighted the

951   effect of the structural connectivity constraints on the time courses, as their distances were

952   significantly smaller when structural connectivity was stronger. Additionally, by changing the

953   functional information and keeping the structural connectivity constant, the learning procedure is

954   dependent on information from both modalities during the estimation of ICNs.

955   Empirical results from our proposed multi-modal model on real data show that our model (the

956   sfCICA) is more sensitive in detecting functional connectivity in both healthy and schizophrenia

957   groups, compared to the CICA model. Estimated ICNs were significantly more spatially similar

958   (**Figure 7a**) to the reproducible template (NeuroMark template (Du et al., 2020)) for both healthy

959   and schizophrenia subjects. This may enhance the replicability of the components using different

960   datasets (Duda et al., 2023).

961 Moreover, the proposed sfCICA model aims to estimate a unified and integrated brain network

962 using regional functional information instead of FNC as in (Zhu et al., 2021) which is the first time

963 this has been performed in an ICA analysis. Overall, the results in **Figure 7b** showed that the

964 distance of the time courses was smaller, which can be interpreted as more functionally correlated,

965 and hence more uniform ICNs. While considering each ICN specifically (**Figures 8 and 9**), ICNs

966 related to cognitive control (CC), and cerebellum (CB) networks were less constrained. In other

967 words, distance minimization of them was less compared to other ICNs. It is highlighted that

968 overall, they are less structurally connected to other ICNs. For instance, ICNs number 37 and 41

969 in the CC network, represent the weakest connection with CC, SM, and CB networks. Also,

970 consistent with prior findings (Glasser et al., 2016; Van Essen et al., 2019; Wu & Calhoun, 2023),

971 the DM has the largest distances within its network ICNs and the weakest with intra-network such

972 as SC network. These findings suggest the advantages of multi-modal approaches, using a

973 combination of structural and functional features, in facilitating the interpretability of the results

974 which is consistent with previous findings (Glasser et al., 2016; Van Essen et al., 2019).

975 Alternatively, there is a hypothesis that structural connectivity may directly influence FNC, as

976 higher structural connectivity leads to higher FNC (Litwińczuk et al., 2022; Zhao et al., 2023).

977 Statistical analysis on FNC of the estimated multi-modal (sfCICA) ICNs and single model ICNs

978 (CICA) in **Figure 11 (a-b)**, represented no association between the FNCs of the two models in

979 specific domains including SM, AUD, VS, CC, and DM. Interestingly results were following

980 previous findings (Li et al., 2020; Tsai et al., 2019). There is evidence that structural connectivity

981 and FNC have no coupling in SM and VS, which means either structural connectivity is not dense,

982 or it may come from dysfunction characteristics of the SZ subjects accompanied by weaker

983 structural connectivity in SM, anterior cingulum cortex (ACC, related to DM domain) (Li et al.,

41

984   2020). So, our results revealed it in the estimated ICNs features (FNC) using the sfCICA model.

985   Regarding the VS domain, little is known about it, however, it has been shown that the connectivity

986   of the visual system in SZ would be reduced (Reavis et al., 2020) which is consistent with our

987   findings. Overall, findings suggested that integrating multi-modal information to estimate ICNs

988   could help to find more accurate intrinsic functional domains in comparison to single-modality

989   models such as the CICA.

990   Our proposed model (sfCICA) was more sensitive to detecting differences between individuals

991   with schizophrenia patients and healthy controls. In schizophrenia both structural and functional

992   networks are affected (Li et al., 2017; S. Qi et al., 2019), our results showed a broad range of

993   impacted networks. Regarding the FNC matrices (**Figure 13 a-b**), findings are consistent with, and

994   extend, those of prior studies. For example, prior studies have reported dysfunction in the CC

995   network, which was also observed in our statistical results using the single modality CICA model.

996   However, the proposed sfCICA model showed enhanced functional connectivity within the SC

997   network with most of the domains, the CC network with other domains (e.g., visual), and the DM

998   network as well as with SM, AUD, and VS. Overall, these findings suggest that the contribution

999   of structural connectivity information could enhance our ability to identify dysfunctional

1000   connections. Also, ICNs related to memory and higher-order cognitive control functions related to

1001   DM networks have been reported as affected regions in individuals with SZ (Aleman et al., 1999;

1002   Minzenberg et al., 2009; Potkin et al., 2009; S. Qi et al., 2019). Consistent with prior findings our

1003   results show that functional correlations of the DM network are lower for the positive connections

1004   and higher for the negative connections (S. Qi et al., 2019), representing the effectiveness of our

1005   multi-modal model. However, in the proposed model, mostly FNC is higher for healthy compared

1006   to schizophrenia but there exist some ICNs that do not show the same pattern. For example, in

1007   ICNs 8 (of the SM network) and 42 (of the CC network), FNC is higher for schizophrenia.

1008   Compared to previous studies, mostly dysconnectivity occurs in DM and SM networks (Rong et

1009   al., 2023), and FNC increment is observed in these domains.

1010   There exist some limitations in this study which would be interesting to consider in future works.

1011   We selected the model order using a standard ICN template including 53 ICNs (NeuroMark_1.0).

1012   The identified ICNs are restricted to prior spatial maps and are modified spatially and temporally

1013   during the optimization process. However, it might be variable over subjects, which should be

1014   considered in future works. Moreover, the standard template is functionally defined. Our multi-

1015   modal sfCICA model uncovers differences in functional connectivity between regions and their

1016   interactions are affected by structural information. To include differences in spatial maps and

1017   enable the comparability of results, a multi-modal (structural/functional) template would be

1018   needed. In parallel, increasing structural and functional studies highlights the need for a multi-

1019   modal simulator. Our synthetic data are independent and structural information has no impact on

1020   fMRI simulation. It could be beneficial to develop a simulator for generating structurally informed

1021   fMRI data (e.g. perhaps via a copula framework (Silva et al., 2014)). In addition, our current model

1022   starts from fixed networks for the structural connectivity, it would be useful to extend the model

1023   to also allow for adaptive updates to the structural connectivity at the single subject level, similar

1024   to what is occurring with the fMRI data. Existing methods have used structural connectivity as a

1025   deterministic constraint to functional connectivity (Seguin et al., 2022). In contrast, in our work,

1026   we propose a data-driven multi-objective model using structural connectivity constraints to

1027   incorporate these into an ICA model resulting in spatial maps, time courses, and FNC. Our

1028   expectation is that the results would increase our sensitivity to patient vs control differences. Our

1029   suggested model is one of the first tools for directly linking structural connectivity/FNC in a data-

1030 driven analysis. Furthermore, future extensions can be developed that allow the structural

1031 connectivity model to adapt to the functional data in the context of a supervised model, optimizing

1032 structural connectivity/FNC to maximize group differences and then using this in a new dataset to

1033 classify. Other future work could be to use our model with an alternative transformation of the

1034 structural connectivity network. Other future work could be to use our model with an alternative

1035 transformation of the structural connectivity network. Most of the not directly connected regions

1036 have polysynaptic communication (Seguin et al., 2022). One way to guide polysynaptic signals in

1037 structural connectivity/FNC models is by using communication network models (Seguin et al.,

1038 2022). Communication network models are derived from structural connectivity and converse to

1039 the structural connectivity, communication network models are dense (Seguin et al., 2022). One

1040 limitation of data fusion is that the structural connectivity informed FNC may be more complex to

1041 interpret than the FNC estimated from fMRI alone. However, there are also advantages as we point

1042 out, especially in enhancing sensitivity to group differences. One way to address this is to perform

1043 both analyses as we have done. An advantage of the use of the NeuroMark spatially constrained

1044 ICA framework is that the data-driven networks maintain their correspondence with one another

1045 due to the similar spatial priors in both. On the other hand, regions-based structural connectivity

1046 was identified before optimization, and it remains constant during resting-state data acquisition. In

1047 addition, for future works, it might be more informatic to use diffusion spectrum imaging (DSI).

1048 Although time courses and spatial maps are updated, the model can be extended to modify

1049 structural weights throughout the optimization process. Beyond this, we can also incorporate the

1050 dynamics of brain function.

1051

44

5. Conclusion

In this work, we proposed a novel, structural-functional constrained independent component analysis (sfCICA), which incorporates both structural and functional connectivity information, guided by spatial maps to estimate functional networks in the human brain. The main motivation for the proposed model is to allow for structural and functional information to jointly influence the model estimation. The resulting ICNs were more spatially focal, and more synchronized in the sfCICA model compared to the CICA model. In addition, we observed that integrating structural connectivity information in the sfCICA enhances the sensitivity to group differences. The results were consistent with those based on synthetic structural and functional imaging data, with different functional information and noise levels. In sum, our findings demonstrate the effectiveness of the proposed model in both synthetic and real data. The approach applies to the study of a wide range of areas including brain development, aging, healthy control, and mental disorders.

6. Acknowledgment

7. Authors contribution

Mahshid Fouladivanda: Conceptualization; Formal analysis; Investigation; Methodology; Software; Visualization; Writing – original draft; Writing – review & editing. Armin Iraji: Conceptualization; Formal analysis; Writing – review & editing. Lei Wu: Software. Theodorus G.M. van Erp: Resources; Writing – review & editing. Aysenil Belger: Resources. Faris

45

1074   Hawamdeh: Writing – review & editing. Godfrey Pearlson: Writing – review & editing. Vince

1075   Calhoun: Conceptualization; Funding acquisition; Investigation; Methodology; Project

1076   administration; Resources; Software; Writing – review & editing.

References

1078   Aleman, A., Hijman, R., De Haan, E. H., & Kahn, R. S. (1999). Memory impairment in
schizophrenia: a meta-analysis. *American Journal of Psychiatry*, *156*(9), 1358-1366.

1080   Allen, E. A., Erhardt, E. B., Damaraju, E., Gruner, W., Segall, J. M., Silva, R. F., Havlicek, M.,
Rachakonda, S., Fries, J., Kalyanam, R., Michael, A. M., Caprihan, A., Turner, J. A.,
Eichele, T., Adelsheim, S., Bryan, A. D., Bustillo, J., Clark, V. P., Feldstein Ewing, S. W.,
. . . Calhoun, V. D. (2011). A baseline for the multivariate comparison of resting-state
networks. *Front Syst Neurosci*, *5*, 2. https://doi.org/10.3389/fnsys.2011.00002

1085   Amaral, L. A. N., Scala, A., Barthélémy, M., & Stanley, H. E. (2000). Classes of small-world
networks. *Proceedings of the National Academy of Sciences*, *97*(21), 11149-11152.
https://doi.org/doi:10.1073/pnas.200327197

1088   Andersson, J. L. R., & Sotiropoulos, S. N. (2016). An integrated approach to correction for off-
resonance effects and subject movement in diffusion MR imaging. *Neuroimage*, *125*, 1063-
1078. https://doi.org/10.1016/j.neuroimage.2015.10.019

1091   Avants, B. B., Tustison, N., & Song, G. (2009). Advanced normalization tools (ANTS). *Insight j*,
2(365), 1-35.

1093   Babaeeghazvini, P., Rueda-Delgado, L. M., Gooijers, J., Swinnen, S. P., & Daffertshofer, A.
(2021). Brain Structural and Functional Connectivity: A Review of Combined Works of
Diffusion Magnetic Resonance Imaging and Electro-Encephalography. *Front Hum
Neurosci*, *15*, 721206. https://doi.org/10.3389/fnhum.2021.721206

1097   Bassett, D. S., Bullmore, E. T., Meyer-Lindenberg, A., Apud, J. A., Weinberger, D. R., & Coppola,

1098   R. (2009). Cognitive fitness of cost-efficient brain functional networks. *Proceedings of the*

1099   *National Academy of Sciences*, *106*(28), 11747-11752.

1100   https://doi.org/doi:10.1073/pnas.0903641106

1101   Batista-García-Ramó, K., & Fernández-Verdecia, C. I. (2018). What We Know About the Brain

1102   Structure-Function Relationship. *Behav Sci (Basel)*, *8*(4).

1103   https://doi.org/10.3390/bs8040039

1104   Calhoun, V. (2018). Data-driven approaches for identifying links between brain structure and

1105   function in health and disease. *Dialogues in Clinical Neuroscience*, *20*(2), 87-99. <Go to

1106   ISI>://WOS:000442461300002

1107   Calhoun, V. D., & Adalı, T. (2012). Multisubject independent component analysis of fMRI: a

1108   decade of intrinsic networks, default mode, and neurodiagnostic discovery. *IEEE Rev*

1109   *Biomed Eng*, *5*, 60-73. https://doi.org/10.1109/rbme.2012.2211076

1110   Calhoun, V. D., Adali, T., Kiehl, K. A., Astur, R., Pekar, J. J., & Pearlson, G. D. (2006). A method

1111   for multitask fMRI data fusion applied to schizophrenia. *Human Brain Mapping*, *27*(7),

1112   598-610. https://doi.org/10.1002/hbm.20204

1113   Calhoun, V. D., Adali, T., Pearlson, G. D., & Pekar, J. J. (2001). A method for making group

1114   inferences from functional MRI data using independent component analysis. *Hum Brain*

1115   *Mapp*, *14*(3), 140-151. https://doi.org/10.1002/hbm.1048

1116   Calhoun, V. D., & de Lacy, N. (2017). Ten Key Observations on the Analysis of Resting-state

1117   Functional MR Imaging Data Using Independent Component Analysis. *Neuroimaging Clin*

1118   *N Am*, *27*(4), 561-579. https://doi.org/10.1016/j.nic.2017.06.012

1119   Calhoun, V. D., & Sui, J. (2016). Multimodal fusion of brain imaging data: A key to finding the

1120   missing link(s) in complex mental illness. *Biol Psychiatry Cogn Neurosci Neuroimaging*,

1121   *1*(3), 230-244. https://doi.org/10.1016/j.bpsc.2015.12.005

1122   Caprihan, A., Abbott, C., Yamamoto, J., Pearlson, G., Perrone-Bizzozero, N., Sui, J., & Calhoun,

1123   V. D. (2011). Source-based morphometry analysis of group differences in fractional

1124   anisotropy in schizophrenia. *Brain Connect*, *1*(2), 133-145.

1125   https://doi.org/10.1089/brain.2011.0015

1126   Chen, J., Calhoun, V. D., Pearlson, G. D., Perrone-Bizzozero, N., Sui, J., Turner, J. A., Bustillo, J.

1127   R., Ehrlich, S., Sponheim, S. R., Canive, J. M., Ho, B. C., & Liu, J. (2013). Guided

1128   exploration of genomic risk for gray matter abnormalities in schizophrenia using parallel

1129   independent component analysis with reference. *Neuroimage*, *83*, 384-396.

1130   https://doi.org/10.1016/j.neuroimage.2013.05.073

1131   Chu, S.-H., Parhi, K. K., & Lenglet, C. (2018). Function-specific and Enhanced Brain Structural

1132   Connectivity Mapping via Joint Modeling of Diffusion and Functional MRI. *Scientific*

1133   *Reports*, *8*(1), 4741. https://doi.org/10.1038/s41598-018-23051-9

1134   Cook, P. A., Bai, Y., Nedjati-Gilani, S., Seunarine, K. K., Hall, M. D., Parker, G. J. M., &

1135   Alexander, D. C. (2006). Camino: Open-Source Diffusion-MRI Reconstruction and

1136   Processing.

1137   Du, Y., & Fan, Y. (2013). Group information guided ICA for fMRI data analysis. *Neuroimage*,

1138   *69*, 157-197. https://doi.org/10.1016/j.neuroimage.2012.11.008

1139   Du, Y. H., Fu, Z. N., Sui, J., Gao, S., Xing, Y., Lin, D. D., Salman, M., Abrol, A., Rahaman, M.

1140   A., Chen, J. Y., Hong, L. E., Kochunov, P., Osuch, E. A., Calhoun, V. D., & Neuroimaging,

1141   A. D. (2020). NeuroMark: An automated and adaptive ICA based pipeline to identify

1142   reproducible fMRI markers of brain disorders. *Neuroimage-Clinical*, *28*.

1143   https://doi.org/ARTN 102375

1144   10.1016/j.nicl.2020.102375

1145   Duda, M., Iraji, A., Ford, J. M., Lim, K. O., Mathalon, D. H., Mueller, B. A., Potkin, S. G., Preda,

1146   A., Van Erp, T. G., & Calhoun, V. D. (2023). Reliability and clinical utility of spatially

1147   constrained estimates of intrinsic functional networks from very short fMRI scans. *Human*

1148   *Brain Mapping*, *44*(6), 2620-2635.

1149   Erhardt, E. B., Allen, E. A., Wei, Y., Eichele, T., & Calhoun, V. D. (2012). SimTB, a simulation

1150   toolbox for fMRI data under a model of spatiotemporal separability. *Neuroimage*, *59*(4),

1151   4160-4167. https://doi.org/10.1016/j.neuroimage.2011.11.088

1152   Erhardt, E. B., Rachakonda, S., Bedrick, E. J., Allen, E. A., Adali, T., & Calhoun, V. D. (2011).

1153   Comparison of multi-subject ICA methods for analysis of fMRI data. *Hum Brain Mapp*,

1154   *32*(12), 2075-2095. https://doi.org/10.1002/hbm.21170

1155   Fillard, P., Descoteaux, M., Goh, A., Gouttard, S., Jeurissen, B., Malcolm, J., Ramirez-

1156   Manzanares, A., Reisert, M., Sakaie, K., Tensaouti, F., Yo, T., Mangin, J. F., & Poupon,

1157   C. (2011). Quantitative evaluation of 10 tractography algorithms on a realistic diffusion

1158   MR phantom. *Neuroimage*, *56*(1), 220-234.

1159   https://doi.org/10.1016/j.neuroimage.2011.01.032

1160   Genon, S., Reid, A., Langner, R., Amunts, K., & Eickhoff, S. B. (2018). How to Characterize the

1161   Function of a Brain Region. *Trends in Cognitive Sciences*, *22*(4), 350-364.

1162   https://doi.org/10.1016/j.tics.2018.01.010

Glasser, M. F., Coalson, T. S., Robinson, E. C., Hacker, C. D., Harwell, J., Yacoub, E., Ugurbil, K., Andersson, J., Beckmann, C. F., & Jenkinson, M. (2016). A multi-modal parcellation of human cerebral cortex. *Nature*, *536*(7615), 171-178.

Goñi, J., van den Heuvel, M. P., Avena-Koenigsberger, A., Velez de Mendizabal, N., Betzel, R. F., Griffa, A., Hagmann, P., Corominas-Murtra, B., Thiran, J. P., & Sporns, O. (2014). Resting-brain functional connectivity predicted by analytic measures of network communication. *Proc Natl Acad Sci U S A*, *111*(2), 833-838. https://doi.org/10.1073/pnas.1315529111

Groves, A. R., Beckmann, C. F., Smith, S. M., & Woolrich, M. W. (2011). Linked independent component analysis for multimodal data fusion. *Neuroimage*, *54*(3), 2198-2217. https://doi.org/10.1016/j.neuroimage.2010.09.073

He, X., & Niyogi, P. (2003). Locality preserving projections. *Advances in neural information processing systems*, *16*.

Honey, C. J., Sporns, O., Cammoun, L., Gigandet, X., Thiran, J. P., Meuli, R., & Hagmann, P. (2009). Predicting human resting-state functional connectivity from structural connectivity. *Proceedings of the National Academy of Sciences*, *106*(6), 2035-2040. https://doi.org/doi:10.1073/pnas.0811168106

Hyvarinen, A. (1999). Fast and robust fixed-point algorithms for independent component analysis. *IEEE Trans Neural Netw*, *10*(3), 626-634. https://doi.org/10.1109/72.761722

Iraji, A., Calhoun, V. D., Wiseman, N. M., Davoodi-Bojd, E., Avanaki, M. R. N., Haacke, E. M., & Kou, Z. (2016). The connectivity domain: Analyzing resting state fMRI data using feature-based data-driven and model-based methods. *Neuroimage*, *134*, 494-507. https://doi.org/10.1016/j.neuroimage.2016.04.006

1186   Iraji, A., Deramus, T. P., Lewis, N., Yaesoubi, M., Stephen, J. M., Erhardt, E., Belger, A., Ford, J.

1187   M., McEwen, S., Mathalon, D. H., Mueller, B. A., Pearlson, G. D., Potkin, S. G., Preda,

1188   A., Turner, J. A., Vaidya, J. G., van Erp, T. G. M., & Calhoun, V. D. (2019). The spatial

1189   chronnectome reveals a dynamic interplay between functional segregation and integration.

1190   *Hum Brain Mapp*, *40*(10), 3058-3077. https://doi.org/10.1002/hbm.24580

1191   Iraji, A., Faghiri, A., Fu, Z., Kochunov, P., Adhikari, B. M., Belger, A., Ford, J. M., McEwen, S.,

1192   Mathalon, D. H., Pearlson, G. D., Potkin, S. G., Preda, A., Turner, J. A., Van Erp, T. G.

1193   M., Chang, C., & Calhoun, V. D. (2022). Moving beyond the 'CAP' of the Iceberg: Intrinsic

1194   connectivity networks in fMRI are continuously engaging and overlapping. *Neuroimage*,

1195   *251*. https://doi.org/ARTN 119013

1196   10.1016/j.neuroimage.2022.119013

1197   Iraji, A., Faghiri, A., Fu, Z., Rachakonda, S., Kochunov, P., Belger, A., Ford, J. M., McEwen, S.,

1198   Mathalon, D. H., Mueller, B. A., Pearlson, G. D., Potkin, S. G., Preda, A., Turner, J. A.,

1199   van Erp, T. G. M., & Calhoun, V. D. (2022). Multi-spatial-scale dynamic interactions

1200   between functional sources reveal sex-specific changes in schizophrenia. *Netw Neurosci*,

1201   *6*(2), 357-381. https://doi.org/10.1162/netn_a_00196

1202   Iraji, A., Fu, Z., Faghiri, A., Duda, M., Chen, J., Rachakonda, S., DeRamus, T., Kochunov, P.,

1203   Adhikari, B. M., Belger, A., Ford, J. M., Mathalon, D. H., Pearlson, G. D., Potkin, S. G.,

1204   Preda, A., Turner, J. A., Erp, T. G. M. v., Bustillo, J. R., Yang, K., . . . Calhoun, V. D.

1205   (2022). Canonical and Replicable Multi-Scale Intrinsic Connectivity Networks in 100k+

1206   Resting-State   fMRI   Datasets.   *bioRxiv*,   2022.2009.2003.506487.

1207   https://doi.org/10.1101/2022.09.03.506487

1208   Iraji, A., Miller, R., Adali, T., & Calhoun, V. D. (2020). Space: A Missing Piece of the Dynamic

1209   Puzzle. *Trends in Cognitive Sciences*, *24*(2), 135-149.

1210   https://doi.org/10.1016/j.tics.2019.12.004

1211   Jenkinson, M., Beckmann, C. F., Behrens, T. E., Woolrich, M. W., & Smith, S. M. (2012). FSL.

1212   *Neuroimage*, *62*(2), 782-790. https://doi.org/10.1016/j.neuroimage.2011.09.015

1213   Jorge Nocedal, S. J. W. (2006). *Numerical Optimization*. Springer New York, NY.

1214   https://doi.org/https://doi.org/10.1007/978-0-387-40065-5

1215   Keator, D. B., van Erp, T. G. M., Turner, J. A., Glover, G. H., Mueller, B. A., Liu, T. T., Voyvodic,

1216   J. T., Rasmussen, J., Calhoun, V. D., Lee, H. J., Toga, A. W., McEwen, S., Ford, J. M.,

1217   Mathalon, D. H., Diaz, M., O'Leary, D. S., Jeremy Bockholt, H., Gadde, S., Preda, A., . . .

1218   Fbirn. (2016). The Function Biomedical Informatics Research Network Data Repository.

1219   *Neuroimage*, *124*(Pt B), 1074-1079. https://doi.org/10.1016/j.neuroimage.2015.09.003

1220   Kim, Y., Joshi, A. A., Choi, S., Joshi, S. H., Bhushan, C., Varadarajan, D., Haldar, J. P., Leahy,

1221   R. M., & Shattuck, D. W. (2023). BrainSuite BIDS App: Containerized Workflows for

1222   MRI Analysis. *bioRxiv*, 2023.2003.2014.532686.

1223   https://doi.org/10.1101/2023.03.14.532686

1224   Klamroth, K., & Jørgen, T. (2007). Constrained optimization using multiple objective

1225   programming. *Journal of Global Optimization*, *37*, 325-355.

1226   Latora, V., & Marchiori, M. (2001). Efficient Behavior of Small-World Networks. *Physical*

1227   *Review Letters*, *87*(19), 198701. https://doi.org/10.1103/PhysRevLett.87.198701

1228   Li, P., Fan, T.-T., Zhao, R.-J., Han, Y., Shi, L., Sun, H.-Q., Chen, S.-J., Shi, J., Lin, X., & Lu, L.

1229   (2017). Altered brain network connectivity as a potential endophenotype of schizophrenia.

1230   *Scientific reports*, *7*(1), 5483.

1231   Li, P., Jing, R. X., Zhao, R. J., Shi, L., Sun, H. Q., Ding, Z., Lin, X., Lu, L., & Fan, Y. (2020).

1232   Association between functional and structural connectivity of the corticostriatal network

1233   in people with schizophrenia and unaffected first-degree relatives. *J Psychiatry Neurosci*,

1234   *45*(6), 395-405. https://doi.org/10.1503/jpn.190015

1235   Lin, Q. H., Liu, J., Zheng, Y. R., Liang, H., & Calhoun, V. D. (2010). Semiblind spatial ICA of

1236   fMRI using spatial constraints. *Hum Brain Mapp*, *31*(7), 1076-1088.

1237   https://doi.org/10.1002/hbm.20919

1238   Litwińczuk, M. C., Muhlert, N., Cloutman, L., Trujillo-Barreto, N., & Woollams, A. (2022).

1239   Combination of structural and functional connectivity explains unique variation in specific

1240   domains of cognitive function. *Neuroimage*, *262*, 119531.

1241   https://doi.org/10.1016/j.neuroimage.2022.119531

1242   Liu, J., Pearlson, G., Windemuth, A., Ruano, G., Perrone-Bizzozero, N. I., & Calhoun, V. (2009).

1243   Combining fMRI and SNP data to investigate connections between brain function and

1244   genetics using parallel ICA. *Hum Brain Mapp*, *30*(1), 241-255.

1245   https://doi.org/10.1002/hbm.20508

1246   Messé, A., Rudrauf, D., Benali, H., & Marrelec, G. (2014). Relating structure and function in the

1247   human brain: relative contributions of anatomy, stationary dynamics, and non-

1248   stationarities. *PLoS Comput Biol*, *10*(3), e1003530.

1249   https://doi.org/10.1371/journal.pcbi.1003530

1250   Minzenberg, M. J., Laird, A. R., Thelen, S., Carter, C. S., & Glahn, D. C. (2009). Meta-analysis

1251   of 41 functional neuroimaging studies of executive function in schizophrenia. *Archives of*

1252   *general psychiatry*, *66*(8), 811-822.

1253   Mišić, B., Betzel, R. F., de Reus, M. A., van den Heuvel, M. P., Berman, M. G., McIntosh, A. R.,

1254   & Sporns, O. (2016). Network-Level Structure-Function Relationships in Human

1255   Neocortex. *Cereb Cortex*, *26*(7), 3285-3296. https://doi.org/10.1093/cercor/bhw089

1256   Newman, M. E. J. (2006). Modularity and community structure in networks. *Proceedings of the*

1257   *National   Academy   of   Sciences*,   *103*(23),   8577-8582.

1258   https://doi.org/doi:10.1073/pnas.0601602103

1259   Park, H. J., & Friston, K. (2013). Structural and functional brain networks: from connections to

1260   cognition. *Science*, *342*(6158), 1238411. https://doi.org/10.1126/science.1238411

1261   Potkin, S., Turner, J., Brown, G., McCarthy, G., Greve, D., Glover, G., Manoach, D., Belger, A.,

1262   Diaz, M., & Wible, C. (2009). Working memory and DLPFC inefficiency in schizophrenia:

1263   the FBIRN study. *Schizophrenia bulletin*, *35*(1), 19-31.

1264   Poupon, C., Rieul, B., Kezele, I., Perrin, M., Poupon, F., & Mangin, J. F. (2008). New diffusion

1265   phantoms dedicated to the study and validation of high-angular-resolution diffusion

1266   imaging   (HARDI)   models.   *Magn   Reson   Med*,   *60*(6),   1276-1283.

1267   https://doi.org/10.1002/mrm.21789

1268   Power, J. D., Cohen, A. L., Nelson, S. M., Wig, G. S., Barnes, K. A., Church, J. A., Vogel, A. C.,

1269   Laumann, T. O., Miezin, F. M., Schlaggar, B. L., & Petersen, S. E. (2011). Functional

1270   network   organization   of   the   human   brain.   *Neuron*,   *72*(4),   665-678.

1271   https://doi.org/10.1016/j.neuron.2011.09.006

1272   Puxeddu, M. G., Faskowitz, J., Betzel, R. F., Petti, M., Astolfi, L., & Sporns, O. (2020). The

1273   modular organization of brain cortical connectivity across the human lifespan.

1274   *Neuroimage*,   *218*,   116974.

1275   https://doi.org/https://doi.org/10.1016/j.neuroimage.2020.116974

1276   Puxeddu, M. G., Faskowitz, J., Sporns, O., Astolfi, L., & Betzel, R. F. (2022). Multi-modal and

1277   multi-subject modular organization of human brain networks. *Neuroimage*, *264*, 119673.

1278   https://doi.org/https://doi.org/10.1016/j.neuroimage.2022.119673

1279   Qi, S., Sui, J., Chen, J., Liu, J., Jiang, R., Silva, R., Iraji, A., Damaraju, E., Salman, M., & Lin, D.

1280   (2019). Parallel group ICA+ ICA: Joint estimation of linked functional network variability

1281   and structural covariation with application to schizophrenia. *Human Brain Mapping*,

1282   *40*(13), 3795-3809.

1283   Qi, S., Yang, X., Zhao, L., Calhoun, V. D., Perrone-Bizzozero, N., Liu, S., Jiang, R., Jiang, T.,

1284   Sui, J., & Ma, X. (2018). MicroRNA132 associated multimodal neuroimaging patterns in

1285   unmedicated   major   depressive   disorder. *Brain*, *141*(3),   916-926.

1286   https://doi.org/10.1093/brain/awx366

1287   Qi, S. L., Silva, R. F., Zhang, D. Q., Plis, S. M., Miller, R., Vergara, V. M., Jiang, R. T., Zhi, D.

1288   M., Sui, J., & Calhoun, V. D. (2022). Three-way parallel group independent component

1289   analysis: Fusion of spatial and spatiotemporal magnetic resonance imaging data. *Human*

1290   *Brain Mapping*, *43*(4), 1280-1294. https://doi.org/10.1002/hbm.25720

1291   Qi, S. L., Sui, J., Chen, J. Y., Liu, J. Y., Jiang, R. T., Silva, R., Iraji, A., Damaraju, E., Salman, M.,

1292   Lin, D. D., Fu, Z. N., Zhi, D. M., Turner, J. A., Bustillo, J., Ford, J. M., Mathalon, D. H.,

1293   Voyvodic, J., McEwen, S., Preda, A., . . . Calhoun, V. D. (2019). Parallel group ICA plus

1294   ICA: Joint estimation of linked functional network variability and structural covariation

1295   with   application   to   schizophrenia. *Human   Brain   Mapping*, *40*(13),   3795-3809.

1296   https://doi.org/10.1002/hbm.24632

1297   Reavis, E. A., Lee, J., Altshuler, L. L., Cohen, M. S., Engel, S. A., Glahn, D. C., Jimenez, A. M.,

1298   Narr, K. L., Nuechterlein, K. H., Riedel, P., Wynn, J. K., & Green, M. F. (2020). Structural

1299   and Functional Connectivity of Visual Cortex in Schizophrenia and Bipolar Disorder: A

1300   Graph-Theoretic   Analysis.   *Schizophrenia   Bulletin   Open*,   *1*(1).

1301   https://doi.org/10.1093/schizbullopen/sgaa056

1302   Rong, B., Huang, H., Gao, G., Sun, L., Zhou, Y., Xiao, L., Wang, H., & Wang, G. (2023).

1303   Widespread Intra- and Inter-Network Dysconnectivity among Large-Scale Resting State

1304   Networks in Schizophrenia. *J Clin Med*, *12*(9). https://doi.org/10.3390/jcm12093176

1305   Seguin, C., Mansour L, S., Sporns, O., Zalesky, A., & Calamante, F. (2022). Network

1306   communication models narrow the gap between the modular organization of structural and

1307   functional   brain   networks.   *Neuroimage*,   *257*,   119323.

1308   https://doi.org/https://doi.org/10.1016/j.neuroimage.2022.119323

1309   Shile, Q., Calhoun, V. D., van Erp, T. G., Damaraju, E., Bustillo, J., Yuhui, D., Turner, J. A.,

1310   Mathalon, D. H., Ford, J. M., Voyvodic, J., Mueller, B. A., Belger, A., McEwen, S., Potkin,

1311   S. G., Preda, A., Birn, F., Tianzi, J., & Jing, S. (2016). Supervised multimodal fusion and

1312   its application in searching joint neuromarkers of working memory deficits in

1313   schizophrenia. *Annu Int Conf IEEE Eng Med Biol Soc*, *2016*, 4021-4026.

1314   https://doi.org/10.1109/embc.2016.7591609

1315   Shine, James M., Bissett, Patrick G., Bell, Peter T., Koyejo, O., Balsters, Joshua H., Gorgolewski,

1316   Krzysztof J., Moodie, Craig A., & Poldrack, Russell A. (2016). The Dynamics of

1317   Functional Brain Networks: Integrated Network States during Cognitive Task

1318   Performance.   *Neuron*,   *92*(2),   544-554.

1319   https://doi.org/https://doi.org/10.1016/j.neuron.2016.09.018

Silva, R. F., Plis, S. M., Adalı, T., & Calhoun, V. D. (2014). A statistically motivated framework for simulation of stochastic data fusion models applied to multimodal neuroimaging. *Neuroimage*, *102*, 92-117.

Skudlarski, P., Jagannathan, K., Anderson, K., Stevens, M. C., Calhoun, V. D., Skudlarska, B. A., & Pearlson, G. (2010). Brain connectivity is not only lower but different in schizophrenia: a combined anatomical and functional approach. *Biol Psychiatry*, *68*(1), 61-69. https://doi.org/10.1016/j.biopsych.2010.03.035

Stam, C. J., van Straaten, E. C. W., Van Dellen, E., Tewarie, P., Gong, G., Hillebrand, A., Meier, J., & Van Mieghem, P. (2016). The relation between structural and functional connectivity patterns in complex brain networks. *International Journal of Psychophysiology*, *103*, 149-160. https://doi.org/https://doi.org/10.1016/j.ijpsycho.2015.02.011

Suárez, L. E., Markello, R. D., Betzel, R. F., & Misic, B. (2020). Linking Structure and Function in Macroscale Brain Networks. *Trends in Cognitive Sciences*, *24*(4), 302-315. https://doi.org/10.1016/j.tics.2020.01.008

Sui, J., Huster, R., Yu, Q., Segall, J. M., & Calhoun, V. D. (2014). Function-structure associations of the brain: evidence from multimodal connectivity and covariance studies. *Neuroimage*, *102 Pt 1*, 11-23. https://doi.org/10.1016/j.neuroimage.2013.09.044

Sui, J., Pearlson, G., Caprihan, A., Adali, T., Kiehl, K. A., Liu, J., Yamamoto, J., & Calhoun, V. D. (2011). Discriminating schizophrenia and bipolar disorder by fusing fMRI and DTI in a multimodal CCA+ joint ICA model. *Neuroimage*, *57*(3), 839-855. https://doi.org/10.1016/j.neuroimage.2011.05.055

1341   Tsai, Y. H., Liang, X., Yang, J. T., & Hsu, L. M. (2019). Modular organization of brain resting
1342   state networks in patients with classical trigeminal neuralgia. *Neuroimage Clin*, *24*,
1343   102027. https://doi.org/10.1016/j.nicl.2019.102027

1344   Van Essen, D. C., Donahue, C. J., Coalson, T. S., Kennedy, H., Hayashi, T., & Glasser, M. F.
1345   (2019). Cerebral cortical folding, parcellation, and connectivity in humans, nonhuman
1346   primates, and mice. *Proceedings of the National Academy of Sciences*, *116*(52), 26173-
1347   26180.

1348   Vergara, V. M., Yu, Q., & Calhoun, V. D. (2018). A method to assess randomness of functional
1349   connectivity   matrices.   *Journal   of   Neuroscience   Methods*,   *303*,   146-158.
1350   https://doi.org/https://doi.org/10.1016/j.jneumeth.2018.03.015

1351   Wang, Z., Xin, J., Wang, Z., Yao, Y., Zhao, Y., & Qian, W. (2021). Brain functional network
1352   modeling and analysis based on fMRI: a systematic review. *Cogn Neurodyn*, *15*(3), 389-
1353   403. https://doi.org/10.1007/s11571-020-09630-5

1354   Wu, L., & Calhoun, V. (2023). Joint connectivity matrix independent component analysis: Auto-
1355   linking of structural and functional connectivities. *Hum Brain Mapp*, *44*(4), 1533-1547.
1356   https://doi.org/10.1002/hbm.26155

1357   Wu, L., Calhoun, V. D., Jung, R. E., & Caprihan, A. (2015). Connectivity-based whole brain dual
1358   parcellation by group ICA reveals tract structures and decreased connectivity in
1359   schizophrenia. *Hum Brain Mapp*, *36*(11), 4681-4701. https://doi.org/10.1002/hbm.22945

1360   Yeo, B. T., Krienen, F. M., Sepulcre, J., Sabuncu, M. R., Lashkari, D., Hollinshead, M., Roffman,
1361   J. L., Smoller, J. W., Zöllei, L., Polimeni, J. R., Fischl, B., Liu, H., & Buckner, R. L. (2011).
1362   The   organization   of   the   human   cerebral   cortex   estimated   by   intrinsic   functional
1363   connectivity. *J Neurophysiol*, *106*(3), 1125-1165. https://doi.org/10.1152/jn.00338.2011

1364 Zamani Esfahlani, F., Faskowitz, J., Slack, J., Mišić, B., & Betzel, R. F. (2022). Local structure-

1365   function relationships in human brain networks across the lifespan. *Nature*

1366   *Communications*, *13*(1), 2053. https://doi.org/10.1038/s41467-022-29770-y

1367 Zhao, J., Huang, C.-C., Zhang, Y., Liu, Y., Tsai, S.-J., Lin, C.-P., & Lo, C.-Y. Z. (2023). Structure-

1368   function coupling in white matter uncovers the abnormal brain connectivity in

1369   Schizophrenia. *Translational Psychiatry*, *13*(1), 214. https://doi.org/10.1038/s41398-023-

1370   02520-4

1371 Zhu, Q., Yang, J., Xu, B., Hou, Z., Sun, L., & Zhang, D. (2021). Multimodal Brain Network Jointly

1372   Construction and Fusion for Diagnosis of Epilepsy. *Front Neurosci*, *15*, 734711.

1373   https://doi.org/10.3389/fnins.2021.734711

1374